SF 298 MASTER COPY KEEP THIS COPY FOR REPRODUCTION PURPOSES

REPORT DOCUMENTATION PAGE

Form Approved
OMB NO. 0704-0188

1. AGENCY USE ONLY *(Leave blank)*	2. REPORT DATE (original 15JAN95) 16JUNE97	3. REPORT TYPE AND DATES COVERED
		Final Progress; 15AUG90-31JUL94

4. TITLE AND SUBTITLE
Materials Processing and Microstructure Control in High Temperature Ordered Intermetallics

5. FUNDING NUMBERS
DAAL03-90-G-0183

6. AUTHOR(S)
Professor J.H. Perepezko

7. PERFORMING ORGANIZATION NAMES(S) AND ADDRESS(ES)
University of Wisconsin-Madison
Department of Materials Science and Engineering
1509 University Avenue
Madison WI 53706

8. PERFORMING ORGANIZATION REPORT NUMBER

9. SPONSORING / MONITORING AGENCY NAME(S) AND ADDRESS(ES)
U.S. Army Research Office
P.O. Box 12211
Research Triangle Park, NC 27709-2211

10. SPONSORING / MONITORING AGENCY REPORT NUMBER
ARO 28005.1-MS-A

11. SUPPLEMENTARY NOTES
The views, opinions and/or findings contained in this report are those of the author(s) and should not be construed as an official Department of the Army position, policy or decision, unless so designated by other documentation.

12a. DISTRIBUTION / AVAILABILITY STATEMENT
Approved for public release; distribution unlimited.

12 b. DISTRIBUTION CODE
DTIC QUALITY INSPECTED 4

13. ABSTRACT *(Maximum 200 words)*

In the development of high temperature intermetallic systems for structural applications a crucial issue is the formulation of materials processing strategies in order to achieve controlled microstructures that are designed to provide for the required mechanical performance. In the current research an integrated approach that couples processing with microstructure control as guided by the operative phase equilibria has been used to identify several promising intermetallic alloys.

The experimental efforts have focused on three areas involving a coordination of phase equilibria information with solidification processing and a fourth area dealing with reaction analysis during composite processing. In the Ti-Al-Nb ternary system new information on the phase stability at elevated temperature has allowed for the design of an aligned multiphase microstructure. A gradient recrystallization treatment has been devised to yield a unidirectional ($\alpha_2+\gamma$) microstructure. In the Ti-Al-Mo system reaction pathways have been identified that allow for the formation of ductile phase dispersoids in γ-TiAl as part of stable two-phase microstructures. In the second area the selective alloying of $MoSi_2$ has been examined to address low temperature ductility problems. The third area of effort involved the processing of alloys containing $NbCr_2$, Laves phase together with a BCC phase. A new approach to the analysis of solubility in Laves phases has been devised based on solute atom size factor. In Nb-Cr-Mo alloys a new design including a strengthened BCC phase together with the Laves phase has been identified. In the final area a new analysis relating to the effectivenes of diffusion barrier coatings has been formulated to examine Ti based metal matrix composites with Al_2O_3 reinforcements. While diffusion barriers can be effective, there is some question about their overall reliability. Further examination of several alloys especially those with multiphase microstructures and the associated processing methods is warranted.

14. SUBJECT TERMS	15. NUMBER IF PAGES
Intermetallics, Materials Processing, Multiphase Microstructure Aluminides, $MoSi_2$, Laves Phases, Phase Equilibria, Thermal Stability	71
	16. PRICE CODE

17. SECURITY CLASSIFICATION OR REPORT	18. SECURITY CLASSIFICATION OF THIS PAGE	19. SECURITY CLASSIFICATION OF ABSTRACT	20. LIMITATION OF AESTRACT
UNCLASSIFIED	UNCLASSIFIED	UNCLASSIFIED	UL

GENERAL INSTRUCTIONS FOR COMPLETING SF 298

The Report Documentation Page (RDP) is used in announcing and cataloging reports. It is important that this information be consistent with the rest of the report, particularly the cover and title page. instructions for filling in each block of the form follow. It is important to ***stay within the lines*** to meet ***optical scanning requirements.***

Block 1. Agency Use Only *(Leave blank)*

Block 2. Report Date. Full publication date including day, month, and year, if available (e.g. 1 Jan 88). Must cite at least year.

Block 3. Type of Report and Dates Covered. State whether report is interim, final, etc. If applicable, enter inclusive report dates (e.g. 10 Jun 87 - 30 Jun 88).

Block 4. Title and Subtitle. A title is taken from the part of the report that provides the most meaningful and complete information. When a report is prepared in more than one volume, repeat the primary title, add volume number, and include subtitle for the specific volume. On classified documents enter the title classification in parentheses.

Block 5. Funding Numbers. To include contract and grant numbers; may include program element number(s), project number(s), task number(s), and work unit number(s). Use the following labels:

C	- Contract	**PR**	- Project
G	- Grant	**TA**	- Task
PE	- Program Element	**WU**	- Work Unit Accession No.

Block 6. Author(s). Name(s) of person(s) responsible for writing the report, performing the research, or credited with the content of the report. If editor or compiler, this should follow the name(s).

Block 7. Performing Organization Name(s) and Address(es). Self-explanatory.

Block 8. Performing Organization Report Number. Enter the unique alphanumeric report number(s) assigned by the organization performing the report.

Block 9. Sponsoring/Monitoring Agency Name(s) and Address(es). Self-explanatory.

Block 10. Sponsoring/Monitoring Agency Report Number. *(If known)*

Block 11. Supplementary Notes. Enter information not included elsewhere such as; prepared in cooperation with...; Trans. of...; To be published in.... When a report is revised, include a statement whether the new report supersedes or supplements the older report.

Block 12a. Distribution/Availability Statement. Denotes public availability or limitations. Cite any availability to the public. Enter additional limitations or special markings in all capitals (e.g. NORFORN, REL, ITAR).

DOD	- See DoDD 4230.25, "Distribution Statements on Technical Documents."
DOE	- See authorities.
NASA	- See Handbook NHB 2200.2.
NTIS	- Leave blank.

Block 12b. Distribution Code.

DOD	- Leave blank
DOE	- Enter DOE distribution categories from the Standard Distribution for Unclassified Scientific and Technical Reports
NASA	- Leave blank.
NTIS	- Leave blank.

Block 13. Abstract. Include a brief *(Maximum 200 words)* factual summary of the most significant information contained in the report.

Block 14. Subject Terms. Keywords or phrases identifying major subjects in the report.

Block 15. Number of Pages. Enter the total number of pages.

Block 16. Price Code. Enter appropriate price code *(NTIS only).*

Block 17. - 19. Security Classifications. Self-explanatory. Enter U.S. Security Classification in accordance with U.S. Security Regulations (i.e., UNCLASSIFIED). If form contains classified information, stamp classification on the top and bottom of the page.

Block 20. Limitation of Abstract. This block must be completed to assign a limitation to the abstract. Enter either UL (unlimited) or SAR (same as report). An entry in this block is necessary if the abstract is to be limited. If blank, the abstract is assumed to be unlimited.

Table of Contents

I. Introduction

The development of advanced aerospace systems such as energy efficient gas turbine engines with high thrust-to-weight ratios and hypersonic speed systems demands the simultaneous development of structural materials that can withstand aggressive environments at high temperatures. The required materials must possess the necessary mechanical properties to serve as structural members and also exhibit intrinsic chemical and microstructural stability. Ordered intermetallics are a class of materials that form long range ordered crystal structures and have the potential for satisfying these severe requirements [88Fle].

Related to the high temperature ordered nature of intermetallics is a high atomic bonding energy in these systems which tends to yield a high elastic modulus especially at elevated temperatures, high melting point, as well as high strain hardening rate, low self diffusion rate and a high recrystallization temperature. In intermetallics containing aluminum, silicon and chromium, there is also favorable oxidation and corrosion resistance due to the formation of protective films at the outer surfaces. Although these characteristics are very favorable, there are also debits to these materials. The strong bonding energy tends to result in low temperature ductility problems and toughness problems which require new concepts in microstructural design to overcome.

As a result of the recent activity on high temperature alloy development intermetallics including a number of aluminides such as those in the Ti, Fe and Ni systems have received considerable attention. In the development and evaluation of mechanical properties and high temperature structural stability, it has become evident that it is essential to consider also the strong influence of materials processing throughout all stages. One of the most important initial stages is the solidification processing. Since many intermetallics involve peritectic reactions as well as nonstoichiometric compositions, solidification, especially in multicomponent systems, can result in severe segregation. Due to the inherently sluggish diffusion in intermetallic alloys the removal of as cast segregation in ingots by homogenization annealing

can be difficult and may not be feasible in alloys with multiphase constitution. With this in mind an effective strategy to produce homogeneous alloy structures is powder processing and associated with the powder processing are rapid solidification effects including the formation of refined microstructural features and in some cases metastable phases. In a number of high melting temperature ordered intermetallics relatively sluggish crystal growth kinetics are expected to occur and to promote the development of the undercooling required for the nucleation and growth of alternate metastable structures with more rapid solidification kinetics [87Gra]. Although it is not anticipated that metastable phases will survive to the operating temperature in a structural application, it is expected that the decomposition of a metastable phase can provide a useful precursor to the development of the final microstructure. With powder samples an important post solidification processing involves consolidation through hot isostatic pressing (HIP) or other methods. With HIP the possibility of incorporating reinforcement phases in composite form is also an advantage.

Throughout all of the processing operations some of the most fundamental data needed for the development of effective treatments is the relevant phase diagram for the system under consideration. All too often there are examples in the current work of heat treatments and processing operations which appear to have no basis in terms of the phase equilibria of the systems which is often unknown or of questionable reliability. Another crucial piece of information for optimized processing is the recognition that specific microstructural designs are needed to achieve mechanical properties suitable for structural applications at high temperatures. Much progress has been made in this regard [88Eva] and useful composite structures have been made through external processing i.e. the addition of fibers or dispersoids to a powder mix and final consolidation. However, it is also possible to consider the application of mechanics concepts to microstructural design through the development of insitu microstructural transitions to yield multiphase structures with assured stability based on phase equilibria information.

The current research effort involves four major thrust areas. In the first area, the studies on ternary aluminides have been persued toward the development of processing controlled microstructures. The continuing interest in the ternary and higher order titanium aluminides demonstrates a need for basic information regarding the phase equilibria and the stability of certain key alloys. To date, the Ti-Al-Nb system has received a significant amount of attention. The interest in the Ti-Al-Ta system has been developed due in part to the chemical similarity between Nb and Ta. Due to its high melting point, Ta offers a potential increase in the service temperature of these alloys. Similarly, Mo additions have been shown to be most effective in modifying mechanical properties. With this point in mind the discussion is presented to focus on the central features of the principal phase equilibria in several ternary Ti-Al-X (X=Ta, Nb, or Mo) systems. In particular, some of the important similarities and contrasting phase equilibria are examined in ternary titanium aluminide alloys with Ta, Nb, and Mo additions to reveal the opportunities for microstructural manipulation by controlling the processing parameters. The second thrust area has focused upon silicide materials such as $MoSi_2$. Molybdenum disilicide has a very high melting temperature, exceeding that of many aluminides. Its oxidation resistance is due to the formation of a silica layer which acts as a protective film at high temperatures and indeed it is commercially used in high temperature furnace applications [78Sch]. Mechanically, $MoSi_2$ behaves as a metal at high temperatures, but it undergoes a ductile to brittle transition at about 1000^{o}C. This is a disadvantage in the $MoSi_2$ since it becomes brittle at low temperatures. However, processing strategies involving the selective alloying of $MoSi_2$ to induce microstructural transitions offer a possibility of overcoming this problem. The key to the microstructural modification centers on the polymorphic transformation toughening reactions. The third area of focus has centered about the Laves phases. The most abundant class of intermetallic compounds is the Laves phases [36Lav,61Dwi]. Literally hundreds of binary and ternary compounds exists with melting temperatures ranging from 7^{o}C to over 2000^{o}C. These structures have shown promise for a variety of useful non-structural applications by tailoring the alloys with solute additions for optimum property response. There are numerous applications involving nonstructural use i.e. hydride formation and magnetic behavior. Although the Laves phases tend to have a fairly large unit cells and number of atoms, an

important class of the Laves phases is essentially cubic and is basically FCC in its stacking. Recent work has indicated that slip dislocations as well as twinning are possible and in multiphase microstructures consisting of a Laves phase and a BCC matrix, useful ductility has been observed [79Ino]. The fourth thrust area has focused upon the stability of Al_2O_3 reinforcement in a titanium alloy (TIMETAL 21S) matrix. The reinforcement of metals with ceramics causes an increase in strength, stiffness, wear resistance, high temperature strength, and a decrease in weight. At the same time, the chemical compatibility of the matrix material with the reinforcing materials at high temperature is of major concern. Titanium alloys are found to react with Al_2O_3 [73Tre,92Li]. The excessive reaction at the interface can severely degrade the strength of the composite by reducing the in-situ fiber failure strain. The excessive reaction at the interface can also have detrimental effect on the interfacial properties. Most of the current modification strategies to reduce the reaction rate at metal-matrix composite interface depend on the reduction of the diffusion rate by interposing some kind of diffusion barriers [82Meh,88Kie,91Kie]. If the diffusion barriers are chosen properly, they do slow down the diffusion rate significantly. A comprehensive evaluation of the stability of Al_2O_3 in TIMETAL 21S and the suitability of Nb as a diffusion barrier in TIMETAL 21S / Al_2O_3 composite have been examined.

References

[88Fle]. R. L. Fleischer, D. M. Dimiduk and H. A. Lipsitt, "Intermetallic Compounds for Strong High-Temperature Research & Development Center Report 88CRD326, (1988).

[87Gra]. J. A. Graves, J. H. Perepezko, C. H. Ward and F. H. Froes, Scripta Met., vol. 21, p. 567 (1987).

[88Eva]. A. G. Evans, Advances in Ceramics, vol. 15, (1988).

[78Sch]. J. Schlichting, High Temperature-High Pressure, vol. 10, p. 241, (1978).

[36Lav]. F. Laves and H. Witte, Metall., vol. 15, p. 840 (1936).

[61Dwi]. A. E. Dwight, Trans. ASM, vol. 53, p. 479, (1961).

[79Ino]. K. Inoue, T. Kuroda and K. Tachikawa, IEEE Trans.Mag. MAG-15, p. 635 (1979).

[73Tre]. R. E. Tressler, T. L. Moore, and R. L. Crane, J. of Mat. Sci., vol. 8, p. 151, (1973).

[92Li]. X. L. Li, R. Hillel, F. Teyssandier, S. K. Choi, and F. J. J. Van Loo, Acta Met., vol. 40, p. 3149, (1992).

[82Meh]. R. L. Mehan and M. R. Jackson, Ceram. Eng. Sci. Proc., (1982), vol. 3, p. 755.

[88Kie]. R. R. Kieschke and T. W. Clyne, presented at "Sixth World Conference on Titanium," France, (1988).

[91Kie]. R. R. Kieschke, R. E. Somekh, and T. W. Clyne, Acta Met., vol. 39, p. 427, (1991).

II. Research Accomplishments in the TI-Al-X (X = Nb, Mo, and Ta) Systems

Ti-Al-Nb system

Some of the most attractive aluminides from the viewpoint of low density and high temperature potential are those in the Ti-Al system: α_2-Ti_3Al (DO_{19}), γ-TiAl ($L1_0$), η-$TiAl_3$ (DO_{22}) and also in the Nb-Al system: δ-Nb_3Al (A-15) and η-$NbAl_3$ (DO_{22}). In fact a few alloy compositions based upon Ti_3Al with Nb additions have been developed and are being examined in high temperature applications [85Lip]. There have also been several studies [88Str,88Ban,77Sas,89Mur] of some of the phase relationships in α_2 alloys with Nb additions which have revealed that at least two ternary phases, a B2 phase with a CsCl structure and an O phase with an orthorhombic structure are present in this system. Other studies [89Ben] on several ternary alloys have indicated that the B2 phase field may be quite extensive at high temperature and yield alloys which exhibit a variety of decomposition products upon cooling including $B8_2$ and ω structures. The reported investigations on the influence of Nb additions on the phase relations in γ-TiAl alloys have also been quite limited. However, it has been established that Nb substitutes preferentially on the Ti sites in γ-TiAl alloys and α_2-Ti_3Al alloys [87Kon]. In the B2 phase Nb substitutes preferentially on the Al sites [87Ban]. In some of the current studies a systematic examination of the ternary equilibria has been undertaken which involves the mapping of the liquidus surface, the determination of an isothermal section at 1200^{o}C and the investigation of selected isoplethal sections.

An examination of the high temperature phase equilibria in the Ti-Al-Nb system has allowed for the determination of the 1200^{o}C isothermal section (figure 1). The 1200^{o}C isothermal section for the Ti-Al-Nb system has been constructed on the basis of 18 ternary samples, as well as several bulk diffusion couples. Some of the refinements of the previous preliminary diagram [90Per] that are shown in figure 1 include the extension of the bcc phase field over a large composition range, the clarification of the ternary (T2) phase region, and the smoothing of the composition variation of the $\gamma/\gamma+\alpha$ boundary. The development of the

$\alpha_2+\beta$ two-phase alloys based on the Ti-Al-Nb system has shown potential for structural applications. Thus, the focus of alloy development has now shifted to such areas as $\alpha_2+\gamma$ two-phase alloys for high temperature applications and the alloys based on the orthorhombic phase [92Ros] for moderate temperature applications. The characteristic lamellar microstructure of the $\alpha_2+\gamma$ alloys may allow for the fabrication of materials which may behave like composites. Figure 2 shows such a lamellar microstructure consisting of α_2 and γ phases in Ti-47Al-6Nb. Further processing methods like directional crystallization may allow for the uniaxial orientation of the lamellae throughout a component [91Mah].

Near the composition Ti_4Al_3Nb it is of interest to note the presence of an isolated region tentatively identified as α (shown as α^* in figure 1), which is consistent with the thermodynamic modelling results [92Kat] at 1100°C. This is nominally the composition with which the $B8_2$ phase forms at low temperature [90Ben]. This phase field, as shown in figure 1, should not be confused with the previously mentioned T2 phase [90Per]. The T2 phase with a B2 structure has been shown to have resulted from specific alloy quenching and cooling treatments [92Per], and it will not be considered further as an equilibrium phase. In the present study a Ti-38Al-6Nb sample was equilibriated at 1200°C for 165 hours and was then quenched into brine solution. The sample revealed a distinct two-phase microstructure (figure 3). Thermal analysis of this sample and another alloy with a nearby composition revealed the presence of a weak endothermic reaction over the temperature range of 1200°C to 1235°C (figure 4). This reaction is likely associated with the formation of the α like (α^*) island.

The importance of the knowledge of an alloy's phase stability can be illustrated by considering the phase equilibria of alloys in the vicinity of the composition Ti-37Al-10Nb. At 1200°C under the equilibrium conditions, these alloys consist of two phases, α^* and B2 (figure 5). Portion of Ti-Al-Nb ternary isothermal section closed to 1200°C is shown in figure 6a. However, on cooling these alloys undergo a series of reactions down to about 1185°C. During this cooling the α phase is transformed to the α_2 phase; a region of the α phase field stabilizes in the vicinity of Ti_4Al_3Nb and separates from the remaining α phase field

[92Kat]. As these transformations are occurring, the α and α_2 phase fields are undergoing compositional shifts to low aluminum concentration. The shift in composition of the α_2 phase field produces a dramatic alteration of the phase equilibria for this region of the ternary system in a temperature range of only about $50^{o}C$. This change in the phase equilibria upon cooling produces a change of almost 90^{o} in the orientation of the tie-lines (figure 6b); the $\alpha+\beta$ two-phase field which is stable at $1200^{o}C$ transforms into the $\alpha_2+\gamma$ two-phase field below $1185^{o}C$.

A systematic study utilizing thermal analysis and then coupling the results with a variety of heat treatments will allow for the determination of the boundaries of the stable phase regions over a range of temperature. Such an analysis may allow for the establishment of processing schedules which can be used to avoid unwanted low temperature phases or reactions. Subsequent heat treatment can be used to dissolve the low temperature precipitates; however a complete removal may become a rather difficult and time consuming task. It is prudent to avoid such problems in the first place if at all possible. In addition to establishing processing schedules, knowledge of the phase equilibria may allow for the retention of the desired phase mixture through the appropriate addition of alloying elements. An example of the importance of the knowledge of the phase stability of such an alloy can be appreciated by examining alloys in the β/B2 phase region near the composition Ti_4Al_3Nb where the $B8_2$ phase is known to form [92Ben]. An example of the formation of low temperature phase(s) can be seen in figure 7a. The sample (Ti-30Al-18Nb) was subjected to a β solutionizing treatment, at $1300^{o}C$ for 24 hours, followed by slow furnace cooling. A subsequent heat treatment at $1200^{o}C$ for 24 hours followed by brine solution quenching was unable to fully remove the precipitates from the sample (figure 7b). Although significantly long annealing time will eventually dissolve the precipitates, a slow cooling from the annealing temperature will result in their re-precipitation. Low temperature phases like $B8_2$ can only be avoided by rapid quenching, and thus the actual phase equilibria at elevated temperatures can only be studied in these samples.

References:

[85Lip]. H. A. Lipsitt, Mat. Res. Soc. Symp. Proc., p. 351, (1985).

[88Str]. R. Strychor, J. C. Williams, and W. A. Soffa, Met. Trans., vol. 19A, p. 1321, (1988).

[88Ban]. D. Banerjee, A. K. Gogia, T. K. nandi, and V. A. Joshi, Acta. Met., vol. 36, p. 871, (1988).

[77Sas]. S. M. L. Sastry and H. A. Lipsitt, Met. Trans., vol. 8A, p. 1543, (1977).

[89mur]. K. Muraleedharan and D. Banerjee, Met. Trans., vol. 20A, p. 1139, (1989).

[89Ben]. L. A. Bendersky and W. J. Boettinger, Mat. Res. Soc. Symp. Proc., vol. 133, p. 45, (1989).

[87Kon]. D. G. Konitzer, I. P. zones, and H. L. Fraser, Scripta Met., vol. 20, p. 265, (1987).

[87Ban]. D. Banerjee, T. K. Nandi, and A. K. Gogia, Scripta Met., vol. 21, p. 597, (1987).

[90Per]. J. H. Perepezko, Y. A. Chang, L. E. Seitzman, J. C. Lin, N. R. Bonda, T. J. Jewett, and J. C. Mishurda, in *High Temperature Aluminides and Intermetallics*, eds. S. H. Whang, C. T. Liu, D. P. Pope, J. O. Stiegler, TMS, Warrendale, PA, p. 19, (1990).

[91Row]. R. G. Rowe, in *Microstructure/Property Relationships in Titanium Aluminides and Alloys*, eds. Y-W. Kim and R. R. Boyer, TMS, Warrendale, PA, p. 387, (1991).

[91Mah]. R. Mahapatra, E. W. Lee, J. Waldman, and J. H. Perepezko, in *Low Density, High Temperature Powder Metallurgy Alloys*, eds. W. E. Frazier, M. J. Koczak, and P. W. Lee, TMS, Warrendale, PA, p. 71, (1991).

[92Kat]. U. R. Kattner and W. J. Boettinger, Mat. Sci. & Engg., vol. A 152, p. 9, (1992).

[90Ben]. L. A. Bendersky, W. J. Boettinger, B. P. Burton, F. S. Biancaniello, and C. B. Shoemaker, Acta Met., vol. 38, p. 931, (1990).

[92Per]. J. H. Perepezko, T. J. Jewett, S. Das, and J. C. Mishurda, in the Proceedings of the 3rd. International SAMPE Metals and Metals Processing Conference, Toronto, Canada, SAMPE, Covina, CA, M357, (1992).

[92Ben]. L. A. Bendersky, in the Proceedings of the 3rd. International SAMPE Metals and Metals Processing Conference, Toronto, Canada, SAMPE, Covina, CA, M346, (1992).

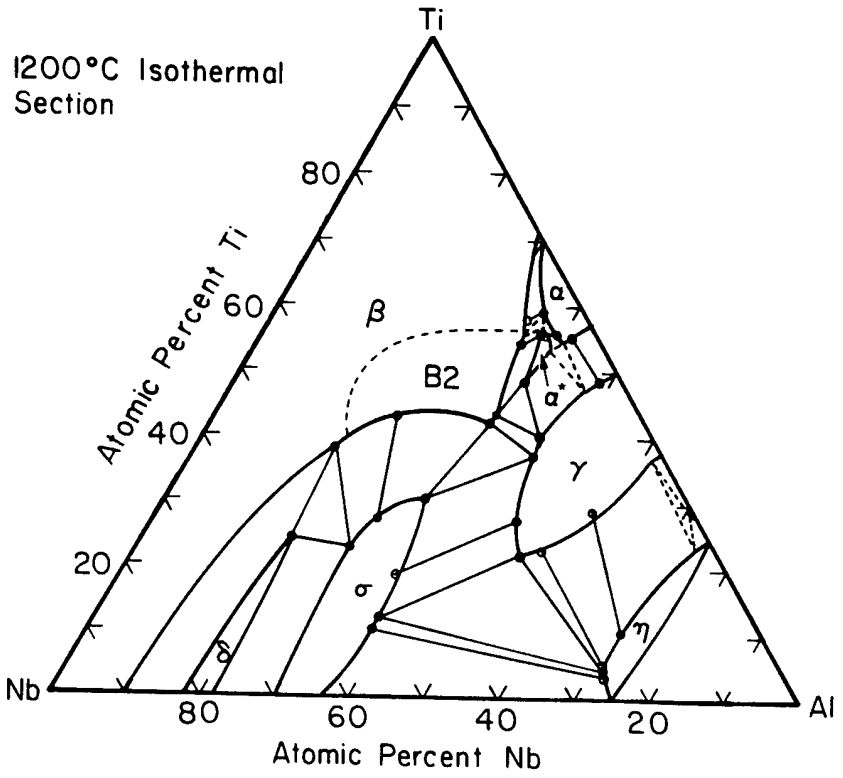

Figure 1. 1200°C isothermal section for the Ti-Al-Nb system.

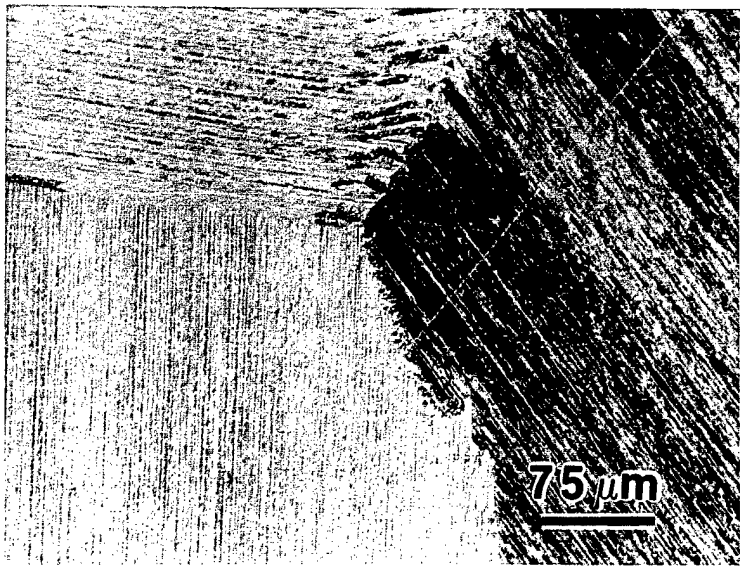

Figure 2. A lamellar microstructure consisting of α_2 and γ phases in Ti-47Al-6Nb.

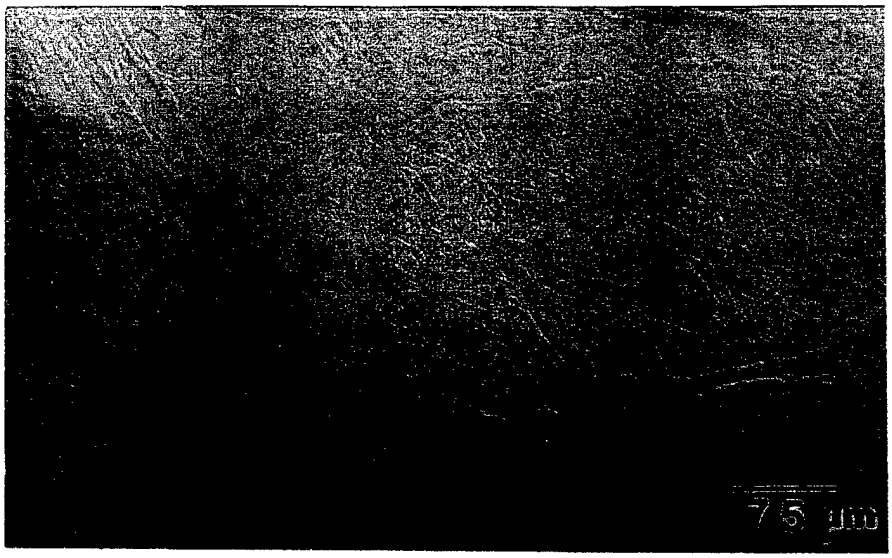

Figure 3. Micrograph of alloy 114 (Ti-38Al-6Nb), etched, annealed at 1200^{o}C for 165 hours then water quenched.

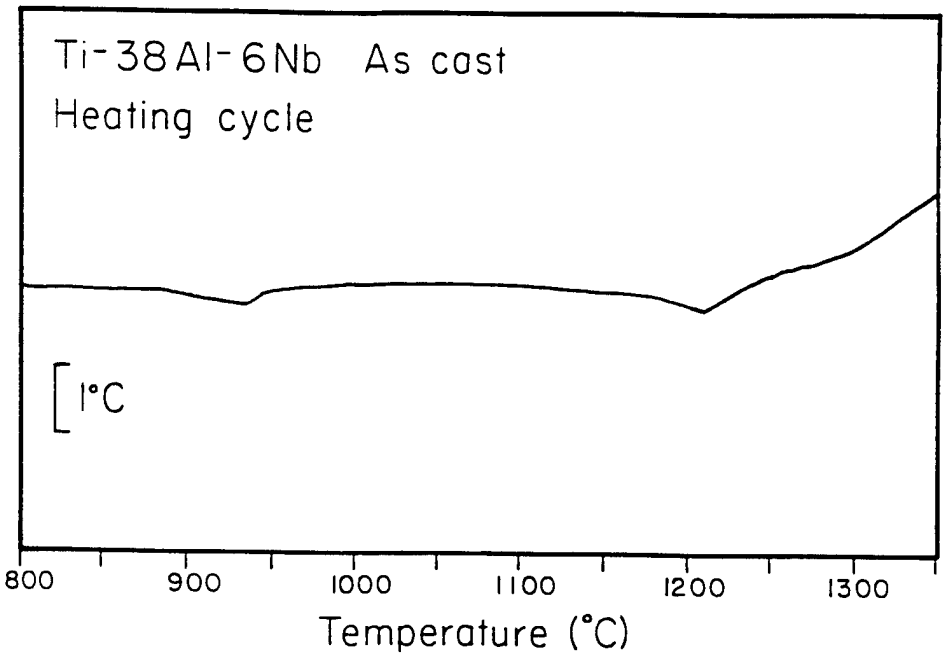

Figure 4. DTA thermogram of alloy 114 (Ti-38Al-6Nb), as cast, heating rate of 30°C/min.

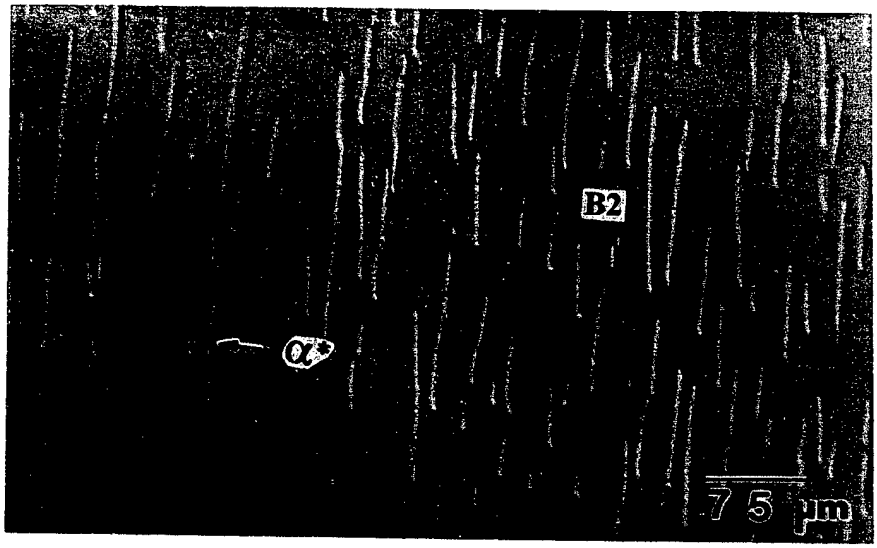

Figure 5. Micrograph of alloy 15 (Ti-37Al-10Nb), etched, annealed 8 days at 1200^{o}C then water quenched, showing a two-phase B2+α* microstructure.

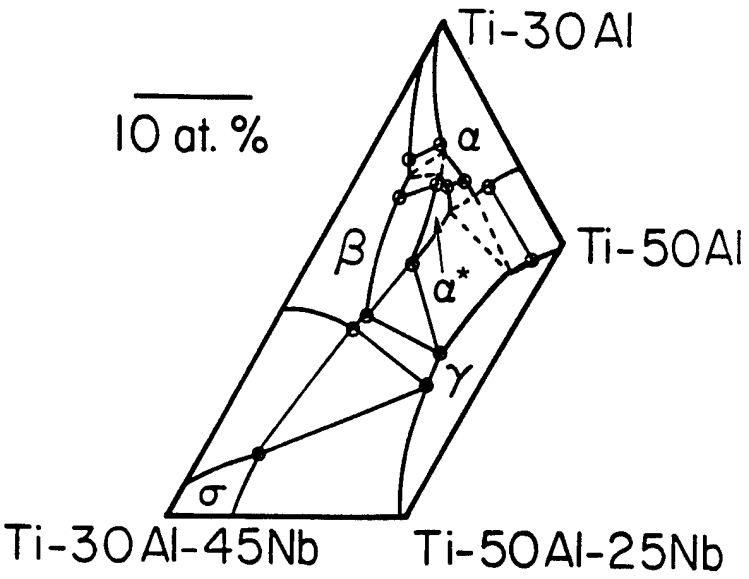

a)

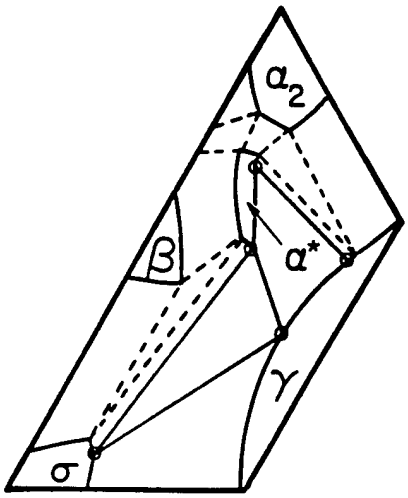

b)

Figure 6. Portions of Ti-Al-Nb ternary isothermal sections closed to (a) 1200°C and (b) 1150°C.

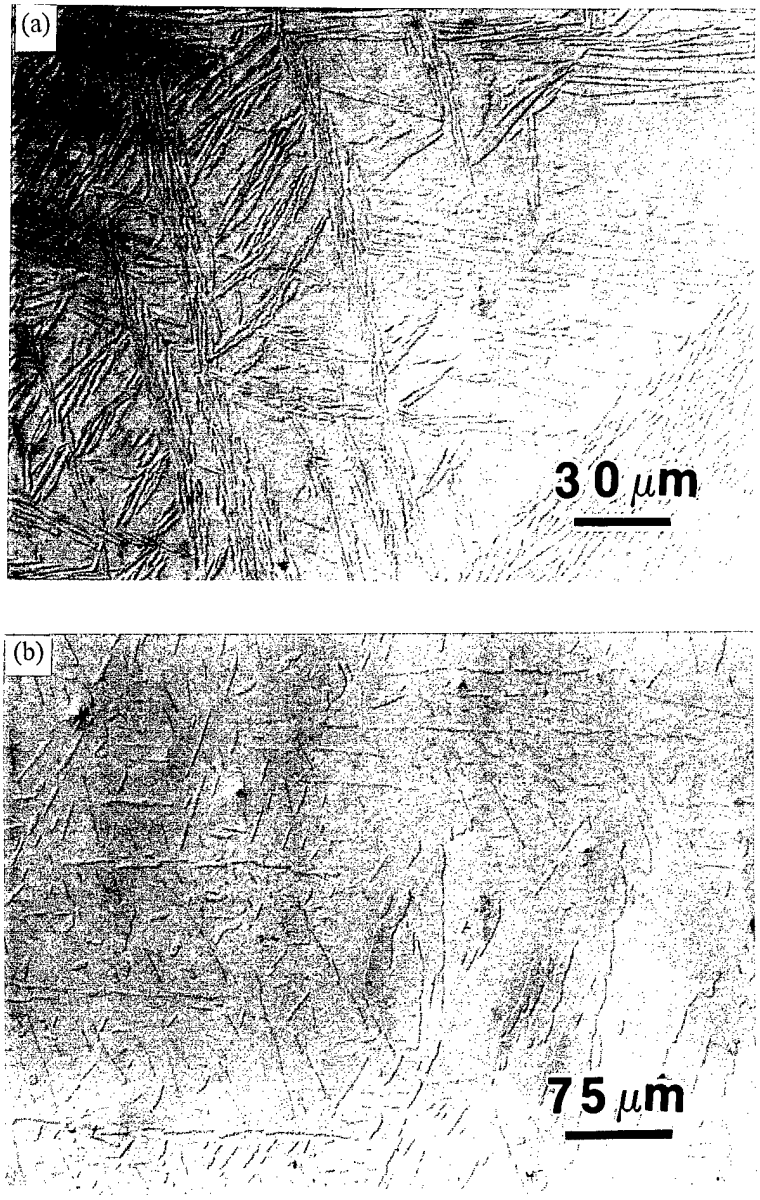

Figure 7. (a) An optical micrograph of Ti-30Al-18Nb subjected to a β solutionizing treatment at 1300^{o}C for 24 hours followed by slow furnace cooling. (b) The effect of a heat treatment at 1200^{o}C for 24 hours followed by brine quenching on the microstructure of figure 7a.

Ti-Al-Ta system

Although good progress has been made in clarifying the binary equilibrium diagrams for the aluminides, especially in the case of the Ti-Al system [89Mis,89McC,91Mis], there are still some questions that remain to be resolved. For example, in the Ta-Al system previous work [73Kim] reported the existence of only two intermetallic phases (Ta_2Al, σ (D8) and $TaAl_3$, η (DO_{22})). However, recent studies indicated the presence of other intermetallic phases with the compositions near TaAl [90Sub], $TaAl_2$ [92Sub], and Ta_2Al_3 [85Sch]. The information on the ternary Ti-Al-Ta system is quite limited. In 1966, Raman [66Ram] proposed an isothermal section at 1000°C revealing an extensive solubility of the β (bcc), σ, α_2 (DO_{19}), and γ ($L1_0$), and a complete solubility of the η binary phases within the ternary system. In 1983, Sridharan and Nowotny [83Sri] reported an isothermal section at 1100°C confirming the extensive solubility into the ternary system of the various binary phases. They also reported the complete miscibility between $TaAl_3$ and $TiAl_3$, but did not consider a third intermetallic in the Ta-Al system between Ta_2Al and $TaAl_3$. In both ternary phase equilibria studies [66Ram,83Sri], no evidence was reported for the development of specific ternary phases. The existence of a ternary phase of ordered bcc (B2 or β_0) structure near the composition Ti-25Al-25Ta was reported by Das et al. [191Das. Another isothermal section that has been examined in the Ti-Al-Ta ternary system is the 1450°C one [91Wea]. The crystal structures of the δ and TaAl phases have been studied by transmission electron microscopy [91McC,92Wea]. The crystal structure of the δ phase has been determined to have a complex bcc type structure with a lattice parameter of about 1.92 nm. The TaAl (ϕ) type phase has yet to be fully characterized; but it is thought to be consisting of a large and complex monoclinic crystal structure [93McC]. Further work by McCullough et al. [91McC[a]] has lead to the determination of the solidification pathways of several alloys in this system. The influence of Ta additions in slowing down diffusional processes and the α_2 layer growth kinetics in several $\beta(Ta_xTi_{1-x})/\gamma$ diffusion couples have been reported [91Das]. A reduction in the α_2 layer growth rate by a factor of about 8 is possible by increasing the amount of Ta. Some of the highlights of the current work are presented below.

1100°C Isothermal Section: An investigation of the 1100°C isothermal section of the Ti-Al-Ta system has indicated extensive solubilities of several phases in the ternary phase fields, as shown in figure 1. These involve the β, B2, α_2, γ, σ, and η phases. The other phases, α (cph), δ, and φ (TaAl type), present at this temperature exhibit narrower or less extensive solubilities than the aforementioned phases. In most cases the boundaries of various phase fields were determined from the quenched samples, but the extent of the β, α, and α_2 phase fields into the ternary diagram were determined from diffusion couple studies. The phase equilibria work, involving both diffusion couple study and bulk alloy sample study, definitely indicates the presence of a ternary phase (B2 or β_0) near the composition Ti-25Al-25Ta. The extent of this B2 phase field has yet to be fully established at 1100°C. However, work to date has shown that the B2 phase field extends at least to the composition of Ti-30Al-20Ta. Transmission electron micrograph and the selected area electron diffraction patterns (SADP) of the B2 phase present in Ti-33Al-20Ta are shown in figure 2. The sample was annealed at 1300°C for 36 hours and then at 1100°C for 120 hours followed by furnace cooling. The ternary phase is indicated in the micrograph as B2. There is some second phase (probably α_2) present in the sample probably due to the alloy composition lying near the ternary phase boundary. The diffraction patterns contain superlattice spots as indicated by arrows. From the subsequent analysis it is clear that the crystal structure of the ternary phase is ordered bcc (B2). The <011> SADP of figure 2 was obtained at a very long exposure time and shows diffuse intensity maxima at **g**=2/3<211> and **g**=1/3<111>. The diffuse intensity maxima arise due to the development of the ordered ω-related phase. The ω-related phase forms as the decomposition product from the B2 phase during aging or slow cooling.

A detailed study on the ordering of the B2 phase in Ti-33Al-17Ta alloy has been published elsewhere [91Das[a]]. Thermal analysis suggests that the ordering of the B2 phase is most likely taking place around 1200°C. To study this transformation samples were annealed at both 1100°C and 1300°C followed by quenching in water. The SADPs obtained from the 1100°C heat treated sample indicate superlattice reflections, and subsequent analysis suggests that they are from the ordered bcc (B2) phase. No antiphase boundary (APB) was found in the microstructure, and this is due to annealing below the ordering

temperature. The APBs have enough time to grow during this annealing treatment, and eventually the whole grain becomes one complete ordered domain. The SADPs obtained from the 1300°C heat treated sample also show superlattice reflections indicating the presence of an ordered bcc phase. The presence of thermal APB in the microstructure of the sample quenched from 1300°C is evident in figure 3. This indeed confirms that the bcc to B2 ordering is taking place between 1100°C and 1300°C as a solid-state transformation [91Das[a],87Cah,91Pra]. Although the sample was quenched from the disordered bcc phase field at 1300°C, the rate of the bcc→B2 ordering reaction is so high that rapid quenching can not arrest this transformation.

This type of order-disorder transformation is most probably of the second-order type [81Por]. It is well known that the second order transformations are not rate limited by nucleation and therefore they do not show any transformation temperature hysteresis due to the change in heating or cooling rate. This simply means that if the heating or cooling rate is changed the second order transformation will take place at the same temperature; therefore, significant undercooling or superheating will not develop at the transformation point. The DTA peak for this transformation in the alloy Ti-33Al-17Ta is present near 1200°C. Figure 4 represents the DTA results showing the effect of heating and cooling rates on the temperature of this order-disorder transformation. It is clear that there is no hysteresis observed for this transformation around 1200°C. It is also known that in the case of the first order transformation there is always a two-phase region below the ordering temperature for non-stoichiometric compositions [81Por]. In that case the disordered phase transforms upon change in temperature to a mixture of ordered precipitate and disordered matrix of different composition. But in the case of the second order transformations there is no such two-phase structure existence. The present alloy composition of interest is not perfectly stoichiometric, and no disordered bcc phase is observed in the quenched microstructure. The absence of the disordered bcc phase in the as-quenched microstructure, the evidence of thermal APBs in the B2 phase, and the absence of thermal hysteresis for the order/disorder transformation confirm that the ordering of B2

phase is indeed taking place as a solid-state transformation around 1200°C, and it is most probably a second order transformation.

1440°C Isothermal Section: A composite 1440°C isothermal section is determined by combining the experimental results of the current study with the data of several other research groups [93McC,91Boe,91Wea]. The three-phase fields identified at this temperature include the σ+δ+α, σ+β+α, δ+η+γ, and η+γ+L phase fields. Although only the σ+δ+α and η+γ+L three-phase fields are identified on the diagram (figure 5), other three-phase fields can be extrapolated from the given two-phase tie-lines. An estimation of the σ+β+α and δ+η+α three-phase fields has been omitted from the diagram in order to illustrate more clearly the other known equilibria. The σ+β+α three-phase field is bound by the σ+β and σ+α two-phase tie-lines, as determined in this work. X-ray analysis of the quenched sample (Ti-51Al-31Ta) indicates the presence of β in the sample yielding the σ+α two-phase tie-line, but the β regions of the samples are too small to study by EPMA. The δ+α+η three-phase field is bound by the δ+η and α+η tie-lines, as reported by Weaver et al. [91Wea], and by the σ+α+δ three-phase field, as determined in the present study.

By comparing the 1440°C isothermal section with the 1100°C section, the most striking differences are the changes in the solubilities of the α, β, and γ phases. The most drastic change is the solubility of the α phase which decreases from about 30 at.% Ta at 1440°C to about 10 at.% Ta at 1100°C. At the same time the region of stability for the β phase shifts considerably away from the Al corner of the system, although its general shape remains unchanged. The most significant change in the γ phase between these two temperatures is an expansion of the width of the phase field. Another item to note about the 1440°C isothermal section is the absence of the ϕ phase. Work by McCullough [93McC] indicates that the ϕ phase does not exist at 1440°C, as shown by their σ+δ two-phase tie-line. Quenching and DTA studies of the alloys in this region reveal that the solubility of the ϕ phase into the ternary diagram decreases as the temperature is increased from 1100°C, and it eventually disappears via a peritectoid reaction. At the same

time the δ phase, which has almost no solubility into the ternary diagram at 1100°C, steadily extends into the ternary as the temperature rises.

References:

[89Mis]. J. C. Mishurda, J. C. Lin, Y. A. Chang, and J. H. Perepezko, Mat. Res. Soc. Symp. Proc., vol. 133, p. 57, (1989).

[89McC]. C. McCullough, J. J. Valencia, C. G. Levi, and R. Mehrabian, Acta Met.,vol. 37, p. 1321, (1989).

[91Mis]. J. C. Mishurda and J. H. Perepezko, in *Microstructure / Property Relationships in Titanium Aluminides and Alloys*, eds. Y-W. Kim and R. R. Boyer, TMS, Warrendale, PA, p. 3, (1991).

[73Kim]. H. Kimura, O. Nakano, and T. Ohkoshi, Trans. Natl. Res. Inst. Met. (Jpn.), vol. 16 (1), p. 1, (1973).

[90Sub]. P. R. Subramanian, D. B. Miracle, and S. Mazdiyasni, Met. Trans. A, vol. 21A, p. 539, (1990).

[85Sch]. J. C. Schuster, Z. Metallkde., vol. 76, p. 724, (1985).

[66Ram]. A. Raman, Z. Metallkde., vol. 57, p. 535, (1966).

[83Sri]. S. Sridharan and H. Nowotny, Z. Metallkde., vol. 74, p. 468, (1983).

[91Das]. S. Das, T. J. Jewett, J. C. Lin, and J. H. Perepezko, in *Microstructure/Property Relationships in Titanium Aluminides and Alloys,* eds. Y-W. Kim and R. R. Boyer, TMS, Warrendale, PA, p. 31, (1991).

[91Wea]. M. L. Weaver, S. L. Guy, R. K. Stone, and M. J. Kaufman, Mat. Res. Soc. Symp. Proc., vol. 213, p. 163, (1991).

[91McC]. C. McCullough, J. J. Valencia, C. G. Levi, and R. Mehrabian, "Intermetallic Compounds in the Ti-Al-Ta System," presented at the Physical Metallurgy of Intermetallic Compounds VII: Titanium Aluminides 3, TMS Fall Meeting, October 23, 1991, Cincinnati, OH.

[92Wea]. M. L. Weaver and M. J. Kaufman, Scripta Metallurgica et Materialia, vol. 26, p. 411, (1992).

[93McC]. C. McCullough, University of California, Santa Barbara, private communication.

[91McC[a]]. C. McCullough, J. J. Valencia, C. G. Levi, R. Mehrabian, M. Maloney, and R. Hecht, Acta Metall. et Mater., vol. 39, p. 2745, (1991).

[91Das[a]]. S. Das and J. H. Perepezko, in *Light Weight Alloys for Aerospace Applications II*, eds. E. W. Lee and N. J. Kim, TMS, Warrendale, PA, p. 453, (1991).

[87Cah]. R. W. Cahn, P. A. Siemers, J. E. Geiger, and P. Bardhan, Acta Metall., vol. 35, p. 2737, (1987).

[91Pra]. U. Prakash, R. A. Buckley, and H. Jones, Phil. Mag. A, vol. 64, p. 797, (1991).

[81Por]. D. A. Porter and K. E. Easterling, *Phase Transformations in Metals and Alloys*, Van Nostrand Reinhold Co., New York, (1981).

[91Boe]. W. J. Boettinger, A. J. Shapiro, J. P. Cline, F. W. Gayle, L. A. Bendersky, and F. S. Biancaniello, Scripta Metallurgica et Materialia, vol. 25, p. 1993, (1991).

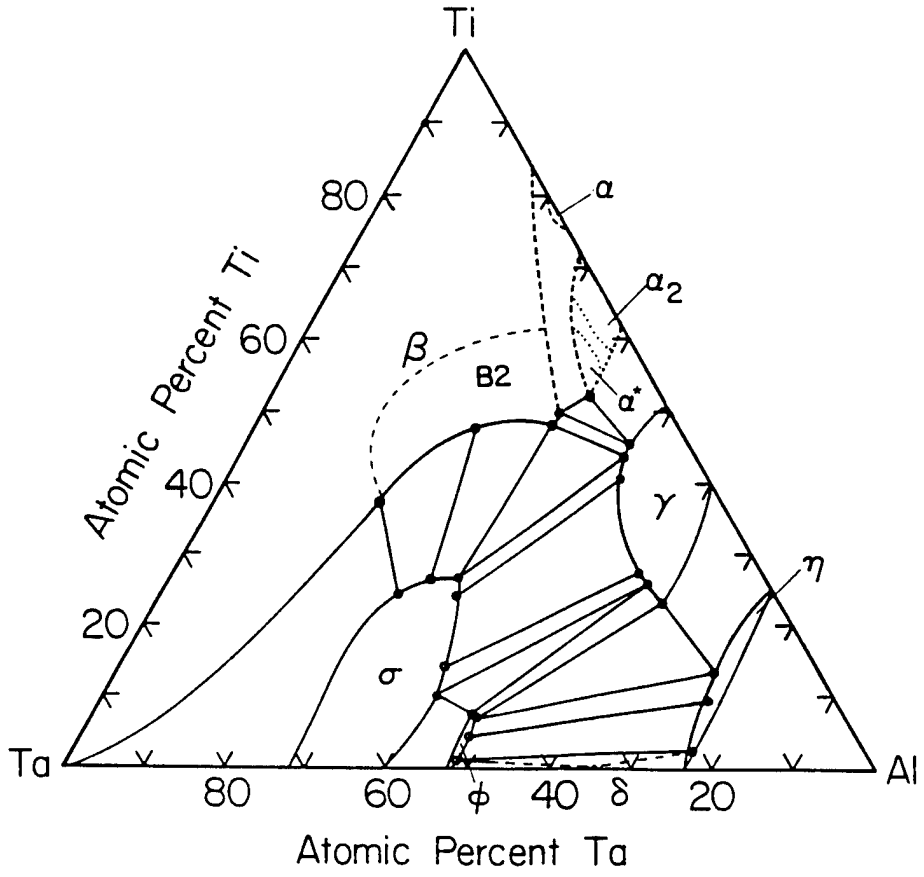

Figure 1. The 1100°C isothermal section of the Ti-Al-Ta system. The estimated three-phase fields in the $\alpha/\alpha_2/\alpha^*/\beta$/B2 regions are omitted for the sake of clarity.

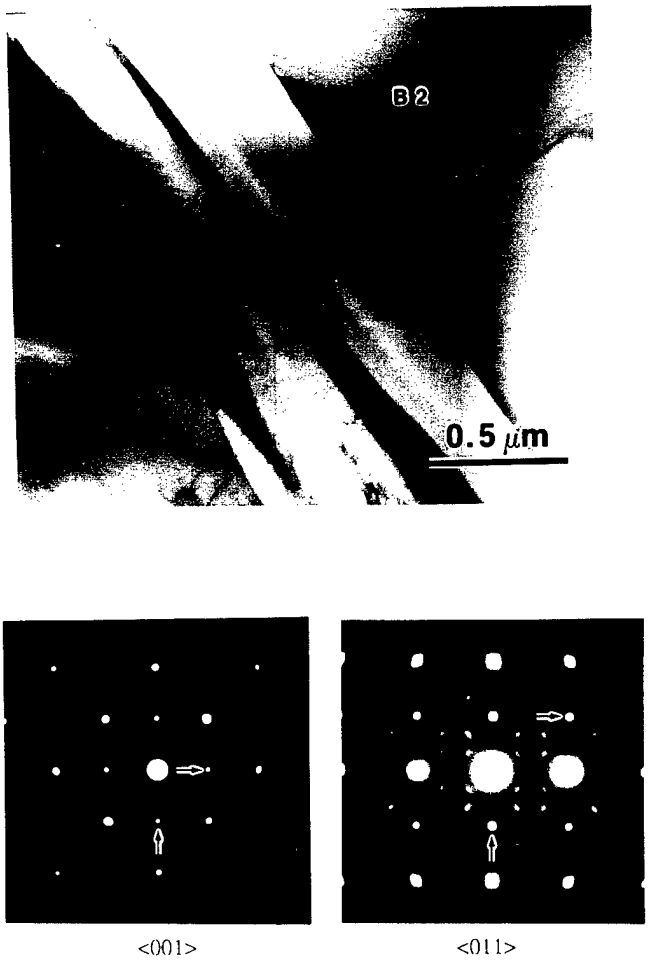

Figure 2. The transmission electron micrograph of Ti-33Al-20Ta and the selected area diffraction patterns obtained from the B2 phase.

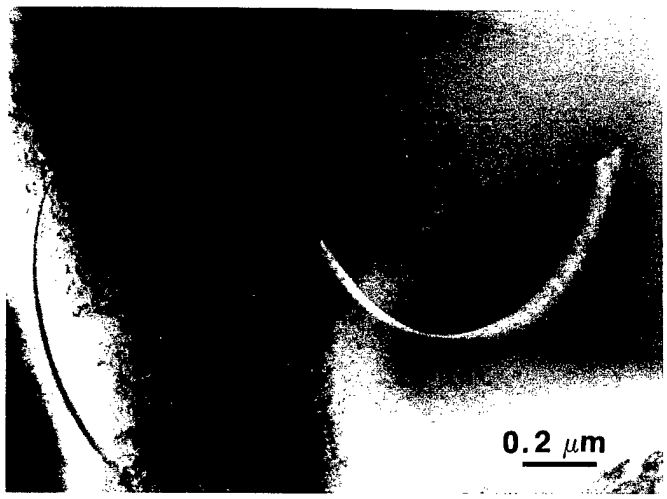

Figure 3. Transmission electron micrograph of the B2 phase in Ti-33Al-17Ta (quenched from 1300^{o}C) showing thermal phase boundary.

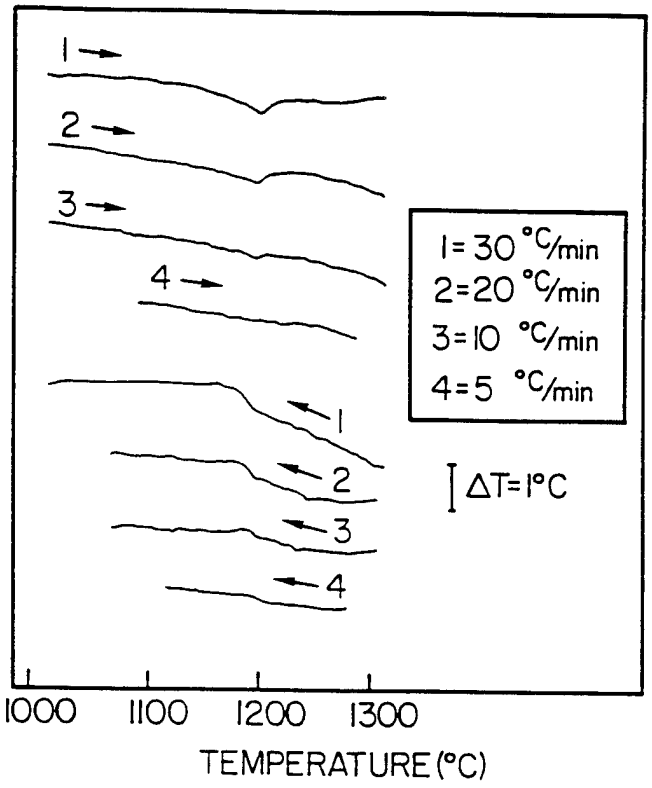

Figure 4. A set of DTA for Ti-33Al-17Ta showing the effect of heating and cooling rates on the temperature of order/disorder transformation.

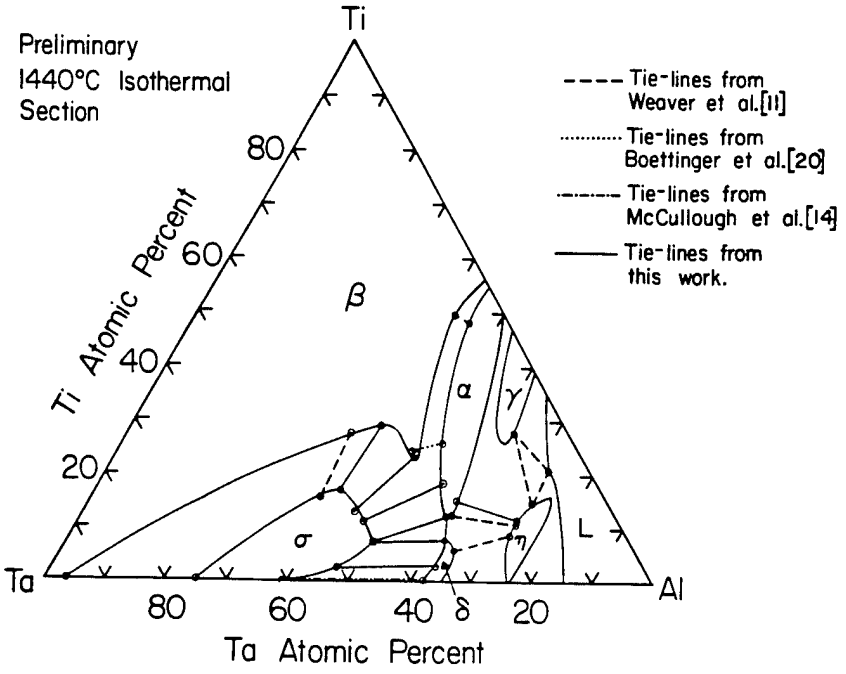

Figure 5. The 1440°C isotharmal section of the Ti-Al-Ta system.

Ti-Al-Mo system

In the development of titanium aluminide alloys for structural applications, the attainment of the most attractive mechanical performance has involved the processing of multiphase alloy compositions. In Ti_3Al based alloys there have been extensive investigations on the influence of α_2 (DO_{19}) and β (A2) or β_o (B2) phase morphologies on mechanical properties [88Str,90Cho]. Similarly, in TiAl based alloys the morphologies of the γ ($L1_0$) and α (A3) or α_2 phases play a key role in the optimization of mechanical properties [91Kim,91Kim[a]]. In order to identify other multiphase microstructural options, the examination of two phase γ and β or β_o alloys is of interest. A consideration of the Ti-Al phase diagram demonstrates that $\gamma+\beta$ two-phase mixtures can not be obtained in binary alloys [91Mis]. However, a review of the literature indicates that ternary additions of beta stabilizing refractory metals such as Cr [91Mas], W [83Mar], Nb [92Per], Ta [92Per], and V [92Shi] can allow for the development of $\gamma+\beta$ microstructures which usually appear with a duplex equiaxed morphology [91Kim,91Kim[a]]. In the current work, the sequence of phase equilibria leading to the development of a γ+B2 microstructure with a new lamellar morphology has been defined in Ti-Al-Mo alloys.

The early work in the Ti-Al-Mo system focussed on the Ti-rich corner of the ternary diagram [54Mar,66Min]. Margolin, Nielson, and Work [54Mar] reported 2 wt.% solubility of Mo in the γ-phase at 1000°C, whereas Ge Dhzhi-Min and Pylaeva [66Min] reported 11.5 wt.% Mo solubility in the γ-phase at the same temperature. Both studies reported 1 wt.% Mo solubility in the α phase and the existence of a $\beta+\gamma$ two-phase field. The presence of the $\beta+\gamma$ two-phase field and the $\alpha+\beta+\gamma$ three-phase field in the ternary diagram were projected from the then accepted binary Ti-Al phase diagram. However, the work of Banerjee, Krishnan, and Vasu [80ban], showed that the difficulties of explaining the observed as-cast microstructures of ternary alloys with $\alpha_2+\gamma$ phases required the existence of a high temperature α-phase field. Banerjee et al. [80Ban] utilized the modified Ti-Al phase diagram by Margolin [73Mar] which contained the high temperature α-phase field, and explained the existence of the $\beta+\gamma$ and $\alpha+\beta+\gamma$ phase fields by a solid-state three-phase equilibrium with a temperature maximum. However, the existence of a

three-phase equilibrium with a temperature maximum would require two separate $\alpha+\beta+\gamma$ three-phase fields, and only one was observed in the regions investigated. The existence of an ordered bcc (B2 or β_O) type structure in the Ti-Al-Mo system at high Mo level near Ti-25Al-25Mo was first identified by Bohm and Lohberg [58Boh]. The two extensive investigations discussed earlier [54Mar,66Min] did not indicate whether the β-phase was ordered in the $\beta+\gamma$ alloys. The TEM investigation by Banerjee et al. [80Ban] did not reveal any B2 ordering. It was suggested that the B2 ordered region did not extend to the β compositions in the $\beta+\gamma$ two-phase alloys investigated. In the current work, the sequence of phase equilibria leading to the development of a $\gamma+\beta_O$ microstructure with a new lamellar morphology has been defined in Ti-Al-Mo alloys.

The optical micrograph in figure 1(a)and the bright-field transmission electron micrograph in figure 1(b) of an annealed (1240^{o}C/150 hours) Ti-50Al-5Mo alloy shows a two-phase lamellar microstructure. X-ray diffraction analysis shows that these two phases are γ and β. The transmission electron microscopy shows that γ-twins are also present in the sample. The XRD results do not reveal any superlattice reflection from the β-phase. In agreement with the analysis given by Bohm and Lohberg [58Boh], a calculation of the size of the ordered peaks indicates that the ordered peak intensity would only be 1 to 2 % of the maximum peak intensity. The electron microdiffraction patterns obtained from the β phase clearly show superlattice reflections indicating ordering of the bcc phase. In order to define more completely the structure of each of the phases present in figure 1(b), a series of electron diffraction experiments was performed (figures 2,3,4, and 5) [93Das]. The point groups of the γ and ordered β (β_O or B2) phases are determined by convergent beam electron diffraction analysis (CBED) as 4/mmm and m~3m, respectively. From the electron diffraction analysis, it can be found that the highest atom density planes of γ and β_O are parallel to each other.

The diffraction analysis clearly identifies that the lamellar microstructure consists of γ and B2 phases, but the morphology is noteworthy since it is the reminiscent of the lamellar α_2 and γ microstructure [91Kim].

An ongoing analysis of the phase equilibria in the Ti-Al-Mo system indicates that the Ti-50Al-5Mo alloy is essentially single phase β at 1400°C, and evolves into an $\alpha+\beta$ two-phase field, an $\alpha+\gamma+\beta$ three-phase region, and then a γ+B2 two-phase field with decreasing temperature. The location of the γ+B2 two-phase field at 1175°C is defined in figure 6, based upon EPMA measurements of phase compositions in the Ti-50Al-5Mo and Ti-45Al-3Mo samples after an annealing treatment of 3 days at 1300°C followed by 6 days at 1175°C. From this sequence of phase equilibria, the high temperature $\alpha+\gamma$ lamellar structure transforms to a B2+γ structure with only a minor change in the γ phase composition and a replacement of the α phase by the B2 phase. As a result, the B2+γ morphology appears to be inherited from a high temperature $\alpha+\gamma$ lamellar structure, and the B2/γ crystallography reflects the $\alpha \rightarrow$B2 transformation. In binary Ti-Al alloys, the $\alpha(\alpha_2)/\gamma$ interfaces are almost fully coherent and exhibit a low mobility [90Mah]. For the B2/γ interfaces in Ti-50Al-5Mo, the misfit along the close packed directions is about 3.5%, based upon the measured lattice parameters. The lamellar B2+γ morphology is relatively stable to a high temperature exposure of 1240°C for 150 hours, but does exhibit some modification at longer times. With controlled thermal-mechanical processing, other non-lamellar B2+γ morphologies may be produced either by treatment at high temperature of the $\alpha+\gamma$ phase mixtures [91kim[a]] and then cooling or by treatment of the $\beta+\gamma$ phase mixtures.

References

[91Mis]. J. C. Mishurda and J. H. Perepezko, in *Microstructure / Property Relationships in Titanium Aluminides and Alloys*, eds. Y-W. Kim and R. R. Boyer, TMS, Warrendale, PA, p. 3, (1991).

[92Per]. J. H. Perepezko, T. J. Jewett, S. Das, and J. C. Mishurda, in the Proceedings of the 3rd. International SAMPE Metals and Metals Processing Conference, Toronto, Canada, SAMPE, Covina, CA, M357, (1992).

[88Str]. R. Strychor, J. C. Williams, and W. A. Soffa, Met. Trans. A, vol. 19A, p. 225, (1988).

[90Ch0]. W. Cho, A. W. Thompson, and J. C. Williams, Met Trans. A., vol. 21A, p. 641, (1990).

[91Kim]. Y-W. Kim, in *Microstructure/Property Relationships in Titanium Aluminides and Alloys*, eds. Y-W. Kim and R. R. Boyer, TMS, Warrendale, PA, 91, (1991).

[91Kim[a]]. Y-W. Kim and D. M. Dimiduk, JOM, vol. 43 (8), p. 40, (1991).

[91Mas]. N. Masahashi, Y. Mizuhara, M. Matsuo, T. Hanamura, M. Kimura, and K. Hashimota, ISIJ International, vol. 31 (7), p. 728, (1991).

[83Mar]. P. L. Martin, M. G. Mendirata, and H. A. Lipsitt, Met. Trans. A, vol. 14A, p. 2170, (1983).

[92shi]. J-D. Shi, Z. Zhong, and D. Zou, Scripta Metallurgica et Materialia, vol. 27, p. 1331, (1992).

[54Mar]. H. Margolin, J. P. Nielson, and H. K. Work, "Titanium Phase Diagram Study," Final Report to Watertown Arsenal Laboratory, Watertown, MA, Contract No. DA-30-069-ORD-208, (1954).

[66Min]. Ge Dhzhi-Min and E. N. Pylaeva, in Titanium and Its Alloys, No. 10, Investigation of Titanium Alloys, Moscow, (1963); English Translation: Israel Program for Scientific Translations, Jerusalem, NASA TT F-362, TT 65-50139, (1966).

[80Ban]. D. Banerjee, R. V. Krishnan, and K. I. Vasu, Met. Trans. A, vol. 11A, p. 1095, (1980).

[73Mar]. H. Margolin, in Metals Handbook, vol. 8, 8th. ed., ASM, Metals Park, OH, p. 264, (1973).

[58Boh]. V. H. Bohm and K. Lohberg, Z. Metallkde., vol. 49 (4), p. 173, (1958).

[93Das]. S. Das, J. C. Mishurda, W. P. Allen, J. H. Perepezko, and L. S. Chumbley, Scripta Metallurgica et Materialia, vol. 28, p. 489, (1993).

[90Mah]. G. J. Mahon and J. M. Howe, Met. Trans. A, vol. 21A, p. 1655, (1990).

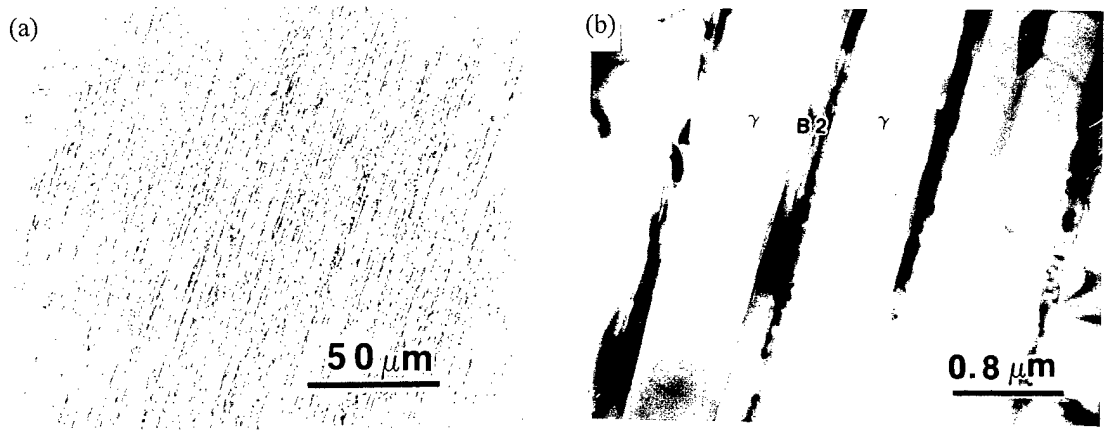

Figure 1. (a) An optical micrograph and (b) a bright-field transmission electron micrograph of an annealed (1240°C/150hours) $Ti_{45}Al_{50}Mo_5$ alloy showing a lamellar microstructure consisting of γ and β_o (B2).

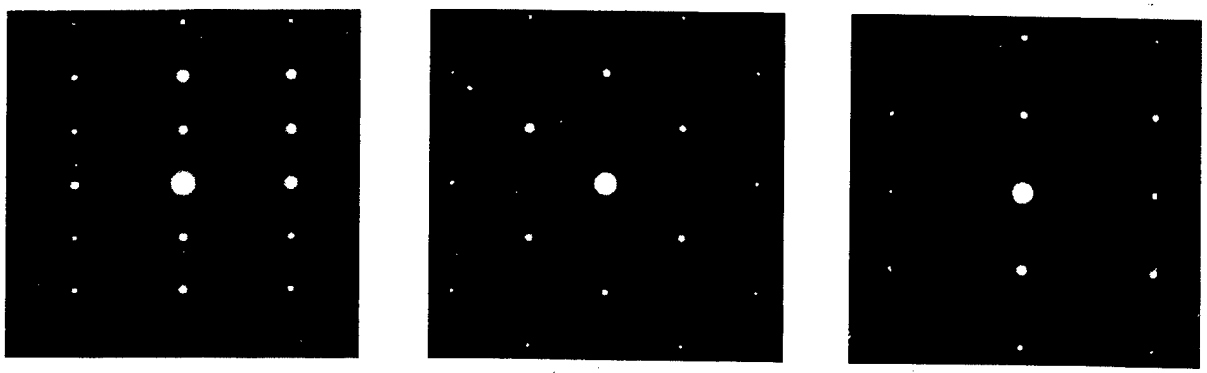

Figure 2. A set of SAD patterns obtained from the γ-phase of figure 1b with the incident electron beam direction parallel to the [100], [011], and [111] zone axes.

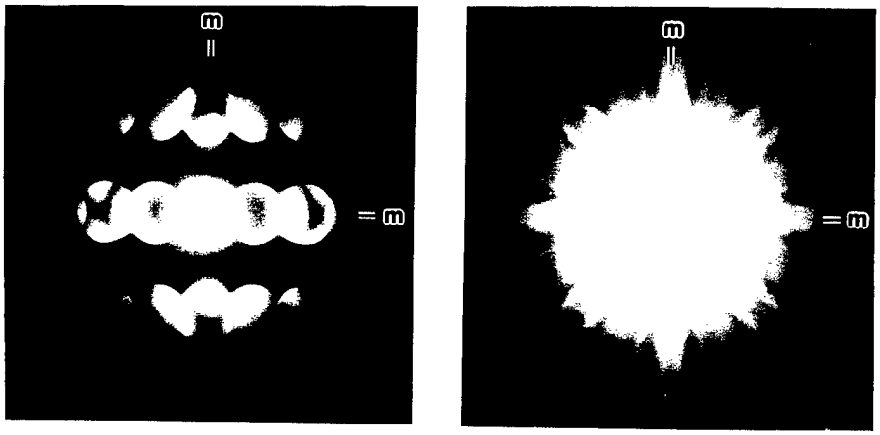

Figure 3. (a) Long and (b) short camera length convergent beam electron diffraction patterns from the [100] zone axis of the γ-phase of figure 1b.

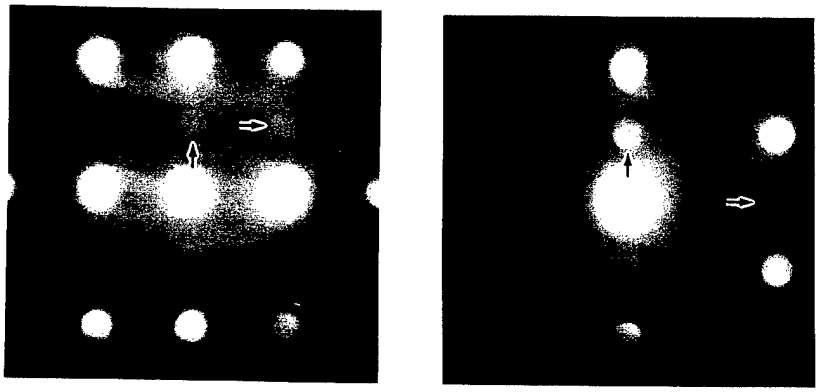

Figure 4. A set of microdiffraction patterns obtained from the β_O phase of figure 1b with the incident electron beam direction parallel to the <011> and <012> zone axes.

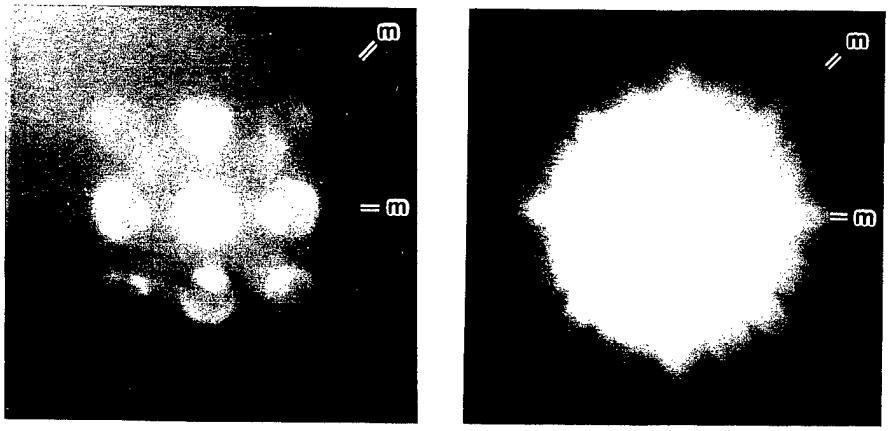

Figure 5. (a) Long and (b) short camera length convergent beam electron diffraction patterns from the <100> zone axis of the β_O phase of figure 1b.

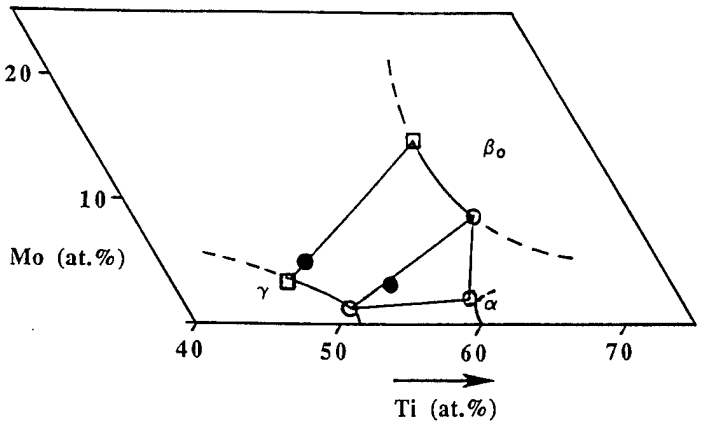

Figure 5. A portion of the 1175^{O}C isothermal section of the Ti-Al-Mo ternary phase diagram. The alloy compositions are indicated by solid circles. The ends of the tie-line and the corners of the tie-triangle are indicated by open squares and circles, respectively.

III. Research Accomplishments in the $MoSi_2$-based Alloys

The successful application of $MoSi_2$-based alloy systems for structural applications at elevated temperatures ($T > 1600^oC$) will require the improvement of mechanical properties without degradation of oxidation resistance or compound thermal stability at high temperature. $MoSi_2$-matrix composite designs have been forwarded to address low temperature toughness and high temperature creep resistance [89Mes]. However, these matrix / composite designs have several metallurgical drawbacks such as dispersoid dissolution, thermal expansion and thermal conductivity mismatch and low oxidation resistance of dispersoids (e.g. TiB_2, SiC, Nb). The application of novel solid solution hardening methods to monolithic $MoSi_2$ based alloys could provide an attractive technological alternative to the matrix / composite approach but has been largely unexploited. $MoSi_2$ undergoes a transition between a high temperature C40 structure to C11b phase at about 1900^oC [72Sve]. The polymorphic transition of $MoSi_2$ offers a new opportunity for microstructure control in this intermetallic that does not appear to have been examined previously. It appears that with modest additions of selected disilicides it will be possible to modify the polymorphic transition temperature, to produce useful level of solid solution strengthening, and to precipitate dispersoids phases without significant degradation of oxidation resistance [76Fit].

$TiSi_2$ - $MoSi_2$:

The pseudobinary $TiSi_2$ - $MoSi_2$ was investigated by Svechnikov et. al.[72Sve] and is shown in figure 1. The $MoSi_2$ rich side of the pseudobinary features intersilicide reactions between hexagonal (C40) disilicide (referred as β-phase) and tetragonal($C11_b$) $MoSi_2$ (referred as t-$MoSi_2$). This crystalline phase sequence is typical of a broad class of transition metal intersilicide reactions. The disilicide crystal structures are composed of the close-packed stacking sequence ABC of (001) planes in the C40 hexagonal structure and the body-centered stacking sequence A^oB^o of (110) planes in the $C11_b$ tetragonal structure. The β-phase exhibits an extensive range of solubility which intersects the $MoSi_2$ terminus above 1860^oC and forms a two phase field (β + t-$MoSi_2$) below 1860^oC. The pseudobinary confirms that relatively small additions of

Ti to $MoSi_2$ stabilize a hexagonal structural form of $MoSi_2$ into ternary solutions. The $TiSi_2$ - $MoSi_2$ pseudobinary system was selected to investigate the perturbation of $MoSi_2$ phase stability resulting from alloying additions and to develop an understanding of C40 -> $C11_b$ intersilicide reactions.

Experiments were conducted on $MoSi_2$ - $TiSi_2$ alloys to resolve conflicting data in the literature. The diagram of figure 1 [72Sve] shows $MoSi_2$ with a polymorphic transition from $C11_b$ to the C40 phase on heating above 1860°C. The $C11_b$ structure has limited solubility of $TiSi_2$ in $MoSi_2$. The diagram shows the C54 form of $TiSi_2$ and a large homogeneity range for the C40 phase. The accuracy of this diagram is suspect because of the large curvature of the boundary between the C40 and (C40 + $C11_b$) phase fields near 1860°C (no heat of transformation data is available to check this slope). The liquidus data are for the C40 phase except near the $TiSi_2$ side of the diagram. There is no liquidus for the $C11_b$ phase because of the supposed polymorphic transformation of the $C11_b$ on heating above 1860°C.

The $MoSi_2$ - $TiSi_2$ quasi-binary diagram was determined in the present work by combining the SEM results and XRD, EDS, and DTA analysis (figure 2). The experiments used to determine this diagram used alloys prepared from research purity elements by arc melting the pure elements in gettered argon with several remelts to ensure homogeneity. A scanning electron micrograph of the arc melt as processed 32Mo-01Ti-67Si alloy (figure 3) shows light contrast primary dendrites with surrounding interdendritic phase. The EDS chemical analysis of the dendrites confirms the primary solid to be $MoSi_2$ and the interdendritic phase to be β-phase. The solidification morphology of β phase suggests that it has formed from the liquid through a peritectic reaction, L + α-$MoSi_2$ = β-$(Ti,Mo)Si_2$. The temperature for the peritectic reaction, liquid + $C11_b$ -> C40, was determined by the heat treatment of samples in gettered helium or argon at successively higher temperatures until an indication of partial melting was observed metallographically after quenching at about 400°C min^{-1}. The liquidus composition at the peritectic temperature was estimated from microprobe data taken from the quenched liquid.

An electron micrograph of an as-cast 25Mo-08Si-67Si alooy is shown in figure 4. The solidification microstructure of arc melt processeed 25Mo-08Ti-67Si alloy displays a three part solidification pathway: primary tetragonal α-$MoSi_2$ dendrites, peritectic formation of β-$(Ti,Mo)Si_2$ and peritectic formation of γ-$(Mo,Ti)Si_2$. The microstructure (figure 4) shows that the primary dendrites of t-$MoSi_2$ are totally enveloped by β-phase. The β-phase, in turn, is completely enveloped by γ-phase which has formed from the last liquid to solidify in the sample. The presence of γ-phase would indicate the liquid composition has proceeded along the liquidus to the peritectic reaction L + β-$(Ti,Mo)Si_2$ = γ-$TiSi_2$. The peritectic temperature for the peritectic reaction, liquid + β-$(Ti,Mo)Si_2$ -> γ-$TiSi_2$, near the $TiSi_2$ side of the diagram, was determined by differential thermal analysis mesurements. The data points shown for the subsolidus regions were determined by microprobe analysis of samples heat treated in gettered helium and quenched at about $400^oC\ min^{-1}$. The very limited solubility of $TiSi_2$ in $MoSi_2$ is confirmed as well as the existence of a wide C40 region in the middle of the diagram. A schematic of the solidification pathway of alloys along the $MoSi_2$-$TiSi_2$ section is shown below:

L = α-$MoSi_2$	$T_m = 2030^oC$
L + α-$MoSi_2$ = β-$(Ti,Mo)Si_2$	$T_p = 1850^oC$
L + β-$(Ti,Mo)Si_2$ = γ-$TiSi_2$	$T_p = 1510^oC$
L = $TiSi_2$	$T_m = 1490^oC$

The $C11_b$ to C40 polymorphic transformation in pure $MoSi_2$:

The experimentally determined $MoSi_2$ - $TiSi_2$ diagram and the solidification path analysis [91Fra] indicates the absence of the $C11_b$ to C40 transformation in pure $MoSi_2$, although a $MoSi_2$ polymorphic transition is shown in the binary Mo-Si system [90Mas]. Figure 5 compares the general shape of the phase boundaries

of the $MoSi_2$ - $TiSi_2$ diagram found in the literature [72Sve] with those measured in the present work. The diagram in the literature contains the polymorphic transformation in pure $MoSi_2$ that gives rise to a two-phase region between C40 and $C11_b$ with $TiSi_2$ additions. The key difference between the diagram in the literature and the revised diagram of this work is an increase in the polymorphic transformation temperature to above the melting point of $MoSi_2$. The upper part of the ($C11_b$ + C40) two-phase field is thus metastable and the peritectic reaction, liquid -> $C11_b$ + C40, is naturally generated. If one were to extrapolate the experimentally measured boundaries of the ($C11_b$ + C40) phase field upward in temperature in the revised $MoSi_2$ - $TiSi_2$ diagram (figure 2), there is no possibility that the boundaries can converge at the $MoSi_2$ terminus axis at a temperature below the melting point of $MoSi_2$ (Tm = 2020^{o}C).

The possible arrangements for the free energy vs. temperature behavior for the liquid, $C11_b$ and C40 phase for pure $MoSi_2$ are shown schematically in figure 6. In this figure the lowest curve at any temperature represents the stable equilibrium phase and the intersections of the free-energy curves correspond to the transition temperatures. If, for pure $MoSi_2$, the $C11_b$ phase transformed to the C40 structure during heating below the melting point, one would have the relationships shown in figure 6(a). On the contrary, if the $C11_b$ structure is stable to the melting point, then the free-energy relationships would exist as in figure 6(b).

$MoSi_2$ - $CrSi_2$:

The ternary alloying of $MoSi_2$ with transition metals (i.e., TM = Nb, Cr, Ti, and Ta) involves the formation of ternary silicide complexes $(Mo,TM)Si_2$ and $(Mo,TM)_5Si_3$ [90Pet]. The ternary alloying of $MoSi_2$ with transition metal additions may add some degree of solid solution strengthening and effect microstructural toughening via methods for second phase precipitation within the $MoSi_2$ matrix.

The solidification microstructure of $MoSi_2$-rich alloys, along the $MoSi_2$-$CrSi_2$ ternary section, displays a two phase mixture of primary $MoSi_2$ ($C11_b$) and intercellular ternary $CrSi_2$ (C40). An example of

solidification morphology of an alloy (5Cr-28Mo-67Si) is shown in figure 7(a). The arc melt processed solidification morphology of $MoSi_2$ displays conformal interfaces indicative of prior liquid/solid interfaces and would suggest the $MoSi_2$ dendrites have formed as a primary solid. The level of Cr solubility in $MoSi_2$ was observed to be 3 atomic percent after thermal annealing.

The $CrSi_2$ terminus side features the formation of a hexagonal ternary disilicide with relatively extensive Mo solution in comparison to the reciprocal solubility behavior exhibited in $MoSi_2$-rich alloys. The chemical analysis of annealed $CrSi_2$-rich alloys (1000°C 400h and 1375°C 98h) would indicate that a continuous series of solid solutions exists between binary $CrSi_2$ and the ternary composition of 17Cr-16Mo-67Si. Therefore, binary $CrSi_2$ exhibits relatively large solubility for Mo. The composition analysis of the solidification microstructures of 25Cr-07Mo-68Si and 29Cr-03Mo-68Si alloys (figure 7(b)) points to a complex solidification pathway which involves the formation of a primary solid $(Cr_x,Mo_{0.33-x})Si_2$, where $0.33 > x > 0.16$, with cellular morphology surrounded by intercellular Si and ($CrSi_2$ + Si) eutectic structure. The solubility of Mo in the annealed $CrSi_2$ ternary phase was observed to be on the order of 16 atomic percent Mo.

This investigation of the response of $MoSi_2$ to ternary additions of Cr corroborates the trend of limited solubility of transition metal additions in the $MoSi_2$ ($C11_b$) crystalline phase. The phase equilibria and lattice parameter trends observed in the $TiSi_2$-$MoSi_2$ and $CrSi_2$-$MoSi_2$ ternary systems would suggest a simple substitution defect mechanism of transition metal solute on the Mo sublattice of the $C11_b$ structure. Table II summarizes the observed levels of transition metal solution in $MoSi_2$ and correlates these solubility trends with interpolated solute Goldschmidt radii for a coordination number of ten. This coordination number reflects the Mo site nearest neighbor environment of the {110} $C11_b$ structure. The atomic size correlation would suggest that a transition metal solute that possesses a smaller Goldschmidt radius than Mo (R_{cn10} = 0.139nm) will have an greater solubility in $MoSi_2$ compared to those solute atoms with a radius equal to or larger than Mo.

These observations of solubility trends with transition metal additions to $MoSi_2$ have served to raise fundamental issues regarding the phase stability of the $C11_b$ crystalline prototype. The $C11_b$ crystalline prototype displays a pronounced bimodal population distribution of the lattice parameter ratio (c_0/a_0) centered about the values of 2.45 and 3.50. The mode at $c_0/a_0 = 3.50$ is primarily composed of noble metal / transition metal pairs such as $CuZr_2$ and $AuHf_2$. The refractory disilicides $MoSi_2$, WSi_2 and $ReSi_2$ reside at lower ratio (c_0/a_0) value of 2.45. The relatively minor changes in the a_0 and c_0 lattice parameters of $MoSi_2$ and WSi_2 with small Cr and Ti additions (Table I) point to an inability of the $C11_b$ disilicide structure to accommodate the lattice perturbation resulting from different size solute atoms.

Summary Remarks

* Solidification pathway along the $MoSi_2$-$TiSi_2$ ternary section can be described by the following reactions:

$L = \alpha\text{-}MoSi_2$ $\quad T_m = 2030^oC$

$L + \alpha\text{-}MoSi_2 = \beta\text{-}(Ti,Mo)Si_2$ $\quad T_p = 1850^oC$

$L + \beta\text{-}(Ti,Mo)Si_2 = \gamma\text{-}TiSi_2$ $\quad T_p = 1510^oC$

$L = TiSi_2$ $\quad T_m = 1490^oC$

* The phase equilibria exhibited in the $MoSi_2$-$TiSi_2$ system lead to the conclusion that there is no C40 high temperatore polymorph in pure $MoSi_2$.

* The solidification pathway of $MoSi_2$ in the ternary sections $MoSi_2$-$TiSi_2$ and $MoSi_2$-$CrSi_2$ initiates with $L = \alpha\text{-}MoSi_2$ ($C11_b$) primary solid. The α-$MoSi_2$ phase exhibits minor solubility for Ti (1 at.%) and Cr (3 at. %) solute additions.

* The lattice parameter ratio (c_0/a_0) at the value of 2.45 apparently represents a characteristic phase stability criterion for $MoSi_2$ ($C11_b$), which is unaffected by the ternary alloying of $MoSi_2$ with Ti and Cr.

The current investigation suggests the phase stability of $MoSi_2$ is primarily controlled by geometrical factors.

References:

[89Mes]. P. J. Meschter and D. S. Schwartz, J. Metals, vol. 41, p. 52, (1989).

[72Sve]. V. N. Svechnikov, Yu. A. Kocherzhinsky and L. M. Yupko, Dokl. Akad. Nauk, Ukrain, RSR, vol. 6A, p. 566, (1972).

[76Fit]. E. Fitzer, J. Schlichting, and F. Schmidt, High-Temperature - High Pressure, vol. 2, p. 553, (1976).

[91Fra]. P. S. Frankwicz and J. H. Perepezko, in "High Temperature Ordered Intermetallics Alloys IV," edited by L. A. Johnson, D. P. Pope and J. O. Stiegler, Mat. Res. Soci. Symp. Proc., vol. 213, p. 169, (1991).

[90Mas]. T. B. Massalski (ed.), in "Binary Alloy Phase Diagrams," ASM, Metals Park, OH, p. 2666, (1990).

[90Pet]. J. J. Petrovic, R. E. Honnell and A. K. Vasudevan, in "Intermetallic Matrix Composites," edited by D L. Anton, P. L. Martin, D. B. Miracle and R. McMeeking Mat. Res. Soci. Symp. Proc., vol. 194, p. 123, (1990) .

[52Now]. H. Nowotny, R. Kieffer, and H. Schachner. Mh. Chem., vol. 83, p. 1243, (1952).

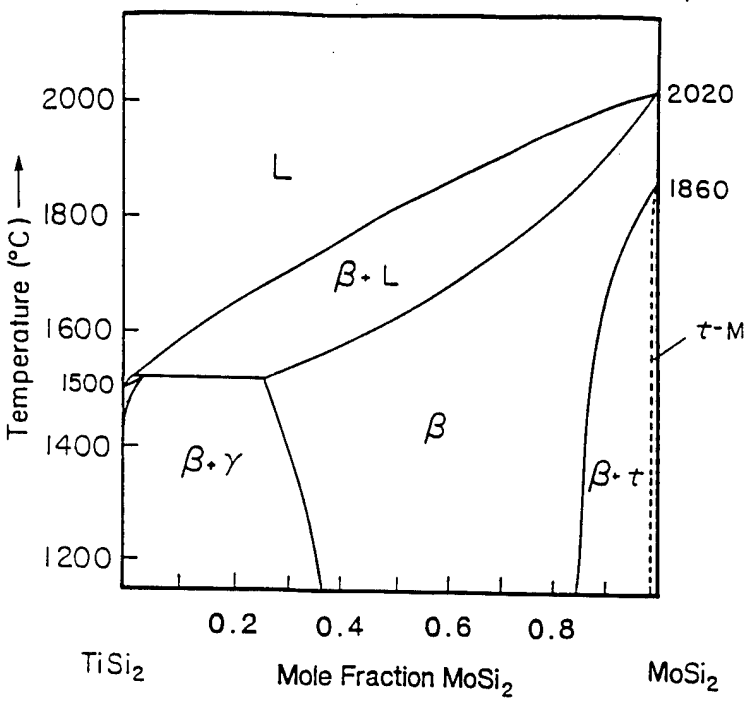

Figure 1. $TiSi_2$ - $MoSi_2$ phase diagram [2].

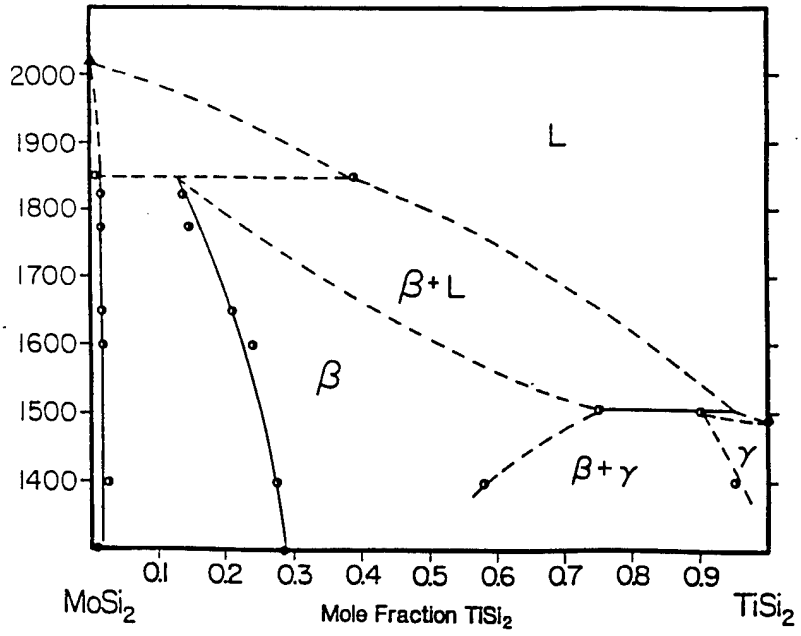

Figure 2. $TiSi_2$ - $MoSi_2$ phase diagram obtained through the present research.

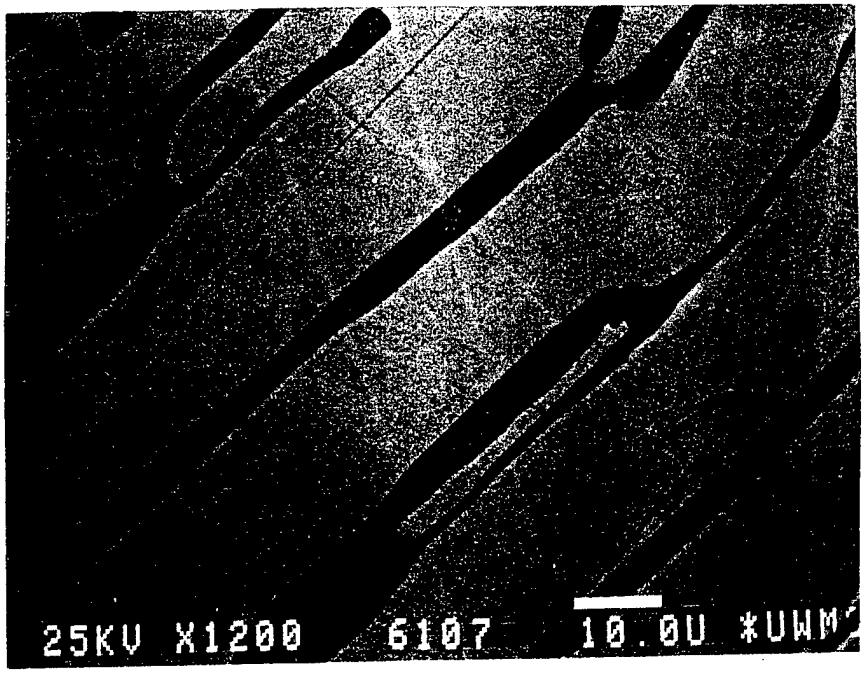

Figure 3. Backscattered scanning electron micrograph of the as-cast alloy, 32Mo-01Ti-67Si (at.%), showing a peritectic structure consisting of primary phase $C11_b$ (light) and interplate C40 phase (dark).

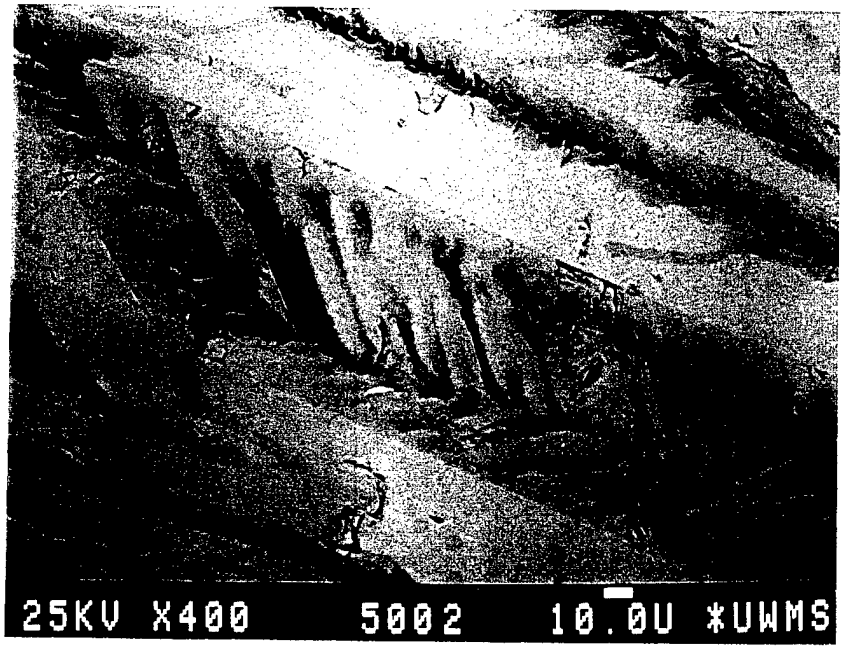

Figure 4. Backscattered electron image of as-cast 25Mo-08Ti-67Si: α-$MoSi_2$ dendrites and interdendritic β-$(Ti,Mo)Si_2$.

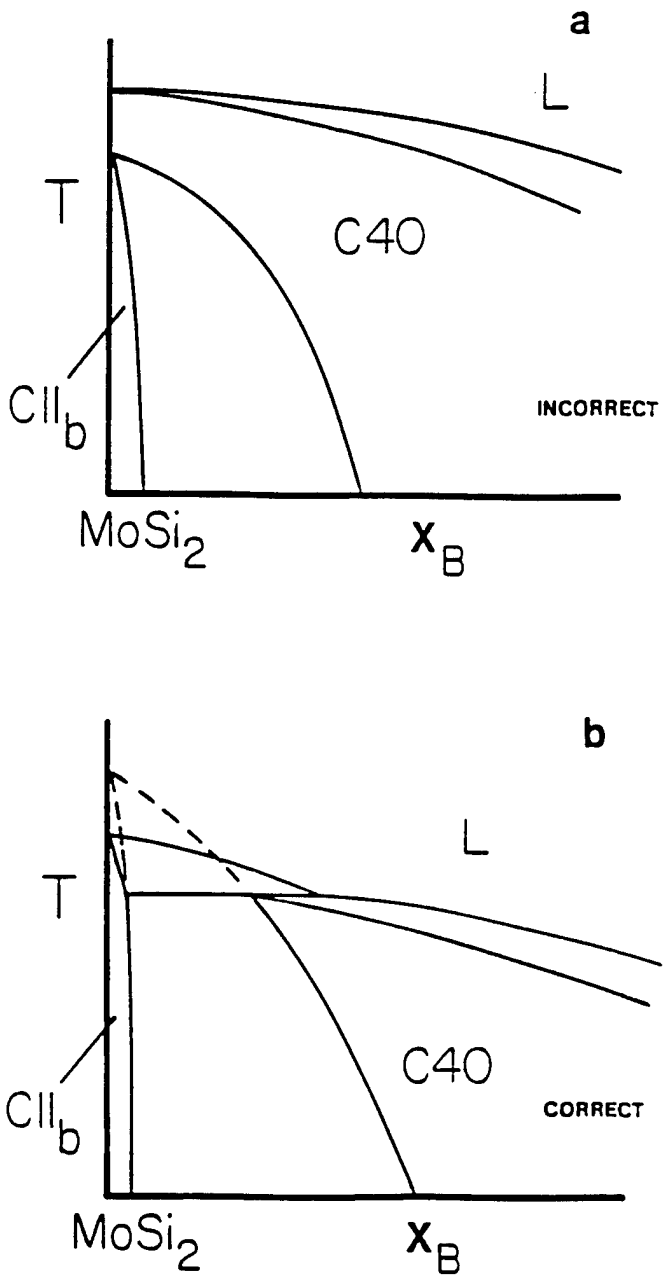

Figure 5. Schematic representation of two possibilities for the $MoSi_2$ - $TiSi_2$ quasi-binary diagram. The polymorphic transformation of pure $MoSi_2$ from $C11_b$ to C40 is (a) below and (b) above the melting point. (b) shows the phase relationships determined in the present study.

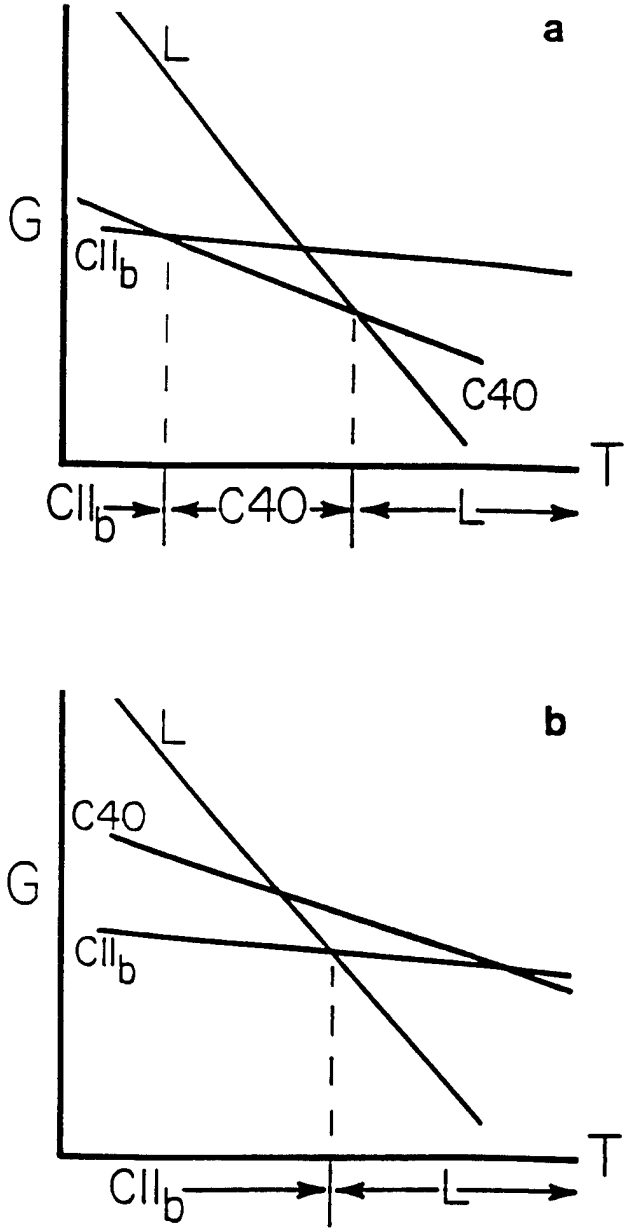

Figure 6. Possible arrangements for the free-energy vs. temperature curves for the liquid, $C11_b$ and C40 phase for pure $MoSi_2$ phase. The polymorphic transformation of pure $MoSi_2$ from $C11_b$ to C40 is (a) below and (b) above the melting point. (b) determined in the present study.

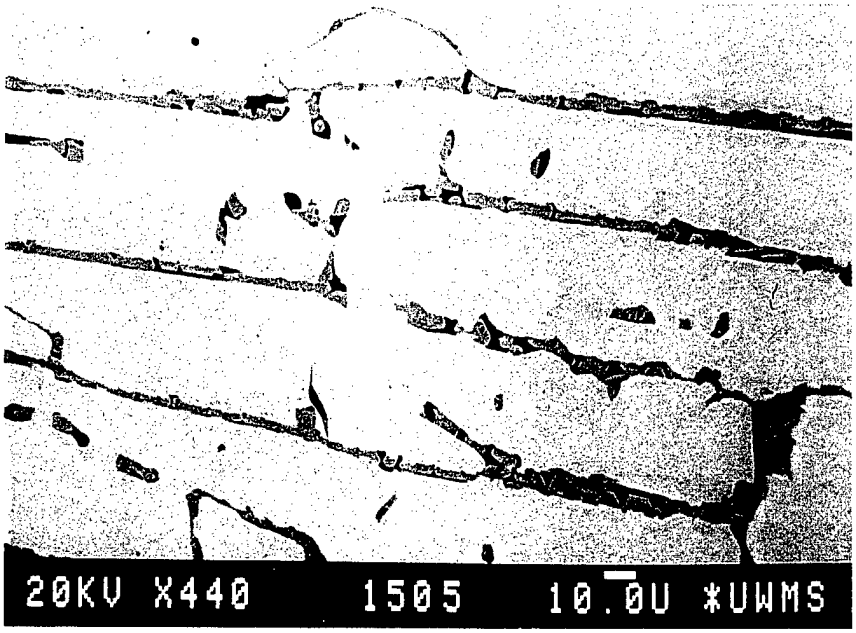

Figure 7(a). Backscattered electron micrograph of as-cast 05Cr-28Mo-67Si. The solidification microstructure displays $MoSi_2$ ($C11_b$) dendrites (light contrast), interdendritic $CrSi_2$ (C40) and Si (dark pores).

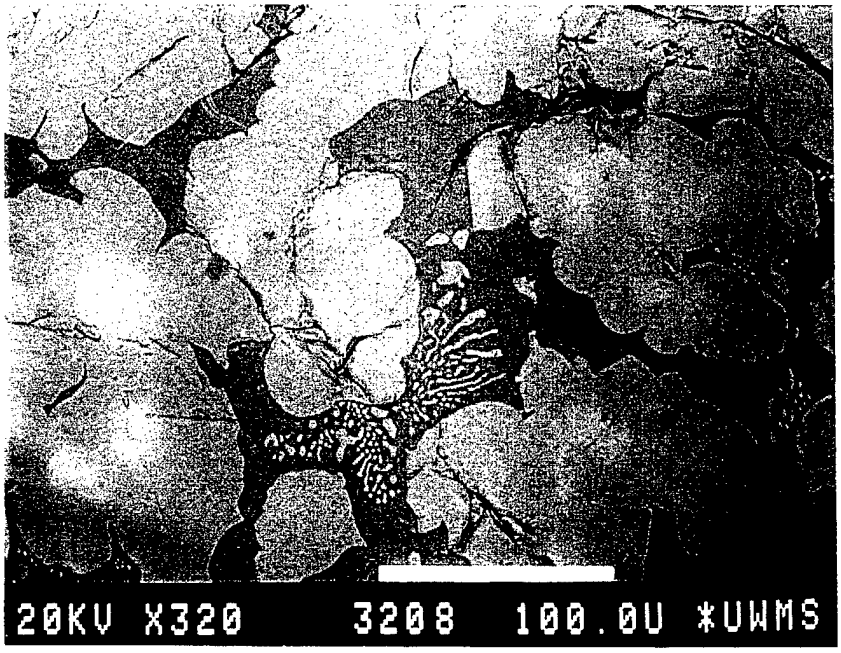

Figure 7(b). Backscattered electron micrograph of 25Cr-07Mo-68Si after cooling at 20°C min^{-1} from the liquid. The solidification microstructures displays ternary $CrSi_2$ cells (light contrast), intercellular Si and areas of ($CrSi_2$ + Si) eutectic morphology.

IV. Research Accomplishments in the Nb-Cr System

Ordered intermetallics often are characterized by sluggish diffusion, resulting in segregated microstructures in compounds forming incongruently from the melt. In fact, even congruent intermetallics are relatively difficult to solidify as homogeneous structures because of the narrow stoichiometry and the likelihood of crystal growth kinetic limitations often associated with ordered metallic compounds. In addition, sluggish diffusion may induce heterogeneous structures with the partial completion of solid state transformations. However, rapid solidification processing (RSP) may offer solidification pathways which not only reduce the extent of segregation during freezing but also may yield metastable precursor microstructures. With novel processing strategies, addvantageous characteristics of intermetallic alloys can be optimized through control of the microstructural evoluton. With these points in mind the processing of the $NbCr_2$ Laves phases has been investigated in the current program.

Several complete phase diagrams have evolved in the current literature on the Nb-Cr system [56Elu,58Ere,59Mis,61Gol,61Pan,65Ell,69Rud,86Ven]. Even though the general features of the phase relationships are similar between each version in the chronology, inconsistencies exist in the reported invariant compositions and solubility limits of the respective phases. The scattering in the published data invokes uncertainty in attaining a reliable determonation of the microstructural development in the binary alloys, especially when comparing the most recent assesment [86Ven] (which is primarily based upon the experimental evaluation in [61Gol]) with other reported compositions for the phase boundaries. Therefore, in an effort to clarify both the phase compositions and relationships in the entire Nb-Cr system, the equilibrium eutectic compositions, solid phase solubilities and lattice parameters have been evaluated in an experimental study. The modified phase diagram as constructed from the experimentally defined eutectic compositions, terminal bcc phase solubilities, solvus biundaries and intermetallic phase field width combined with the experimentally determined temperatures from references [61Pan,69Rud] is shown in figure 1.

The calculated phase diagram (with the estimated T_0 curve) (figure 2) indicates that the development of a metastable bcc solid solution is possible with liquid undercooling levels of 400°C (~0.2 T_m) and the supression of the nucleation and growth of the Laves phase. Indeed the splat quenching was shown to promote compositionaly refined microstructures, and with the high cooling rates, supressed the nucleation and growth of the kinetically sluggish Laves phase to allow liquid undercoolings which favored a disordered bcc phase with more rapid solidification kinetics. An example of the microstructural development in the Cr-rich eutectic splat together with the schematic microstructure and the solidification pathway is shown in figure 3. The cross sectional SEM micrograph (figure 3) of Cr-rich eutectic shows columner bcc grains extending from the surface to the middle of the splat. In the middle of the foil, fine eutectic regions are apparent. The microstructural evolution can be explained by the initial nucleation and growth of a bcc phase from the undercooled melt, and after recalescence, solidification of a liquid composition which lies in the coupled zone of the eutectic.

In addition to the Nb-Cr binary phase equilibria and relationships, the Nb-Cr-Ti ternary phase equilibria at 950°C was defined (figure 4). Titanium was chosen as a ternary alloying addition since it lowers both the density and stacking fault energy as well as potentially broadening the Laves phase solubilty. In addition Ti stabilizes the bcc phase in Nb and Cr alloys. Therefore, an yield of metastable bcc phase in the Nb-Cr-Ti can be expected. Alloys with 10 and 20 at.% Ti additions to $NbCr_2$ are splat quenched, and as the Ti content increased the relative amounts of XRD bcc phase peaks increased with respect to the Laves phase peaks (figure 5). The microstructural development of the two primary phase in the $NbCr_2$+10 at. % Ti alloy is shown in figure 6. Figure 6(a) (top ribbon) illustrates the growth of the bcc phase which was eventually consumed by the Laves phase in the middle of the splat. Figure 6(a) (bottom ribbon) demonstrates the continuous bcc growth across the majority of the splat. However, it appears in both ribbons of the micrograph (figure 6) that a thin layer of the Laves phase originally grew from one of the anvil sides for approximately 3 microns. In figure 6(b), an example of a Laves phase growth front and bcc growth front impinging in the middle of the splat is demonstrated. The $Nbcr_2$+20 at.% Ti alloy indicated a majority of of

bcc phase development across th eentire splat, but some regions of primary Laves phase development from the anvil side could be found (figure 7). Base dupon the isotherm development (figure), the $NbCr_2$ plethal section is schematically illustrated in figure 8. The metastable solidification pathway for for bcc phase development is demonstrated for the 10 and 20 at.% Ti alloys. The metastable extension of the liquid+bcc region (including the dotted T_0) from pure Ti to $NbCr_2$ is show in the schematic diagram. At the composition of the 10 at.% or 20 at.% Ti alloy (C_0), the liquid alloy is undercooled to some extent below the dotted T_0 (line 1). The bcc phase nucleates and grows during recalescence to some unknown temperature in a C14 and/or C15 phase region. Other similar systems such as Nb-Cr Mo show Laves phase+BCC two phase microstructures which show a promising response to solid state reactions to strengthen the BCC phase.

Summary Remarks

* The eutectic compositions, terminal bcc phase solubilities, solvus boundaries and intermetallic phase field width have been experimentally defined, and combined with the experimental temperature measurements from references [61Pan,69Rud] provide a modified equilibrium Nb-Cr phase diagram.

* In the rapid solidification processing extende metastable bcc solid solution have been formed with reduced compositional segregation. The bcc solid solutions form with the immediate or eventual suppression of the kinetically sluggish Laves phase nucleation and/or growth as compared to the disordered bcc phase, depending upon the liquid undercooling at the various stages of solidification in the particular alloy.

* Based upon the correlation of the splat quenched alloys XRD traces and bcc lattice parameters with the defined terminal solution limits and the lattice parameters of the bcc phases in equilibrium processing, the metastable nature of the splat -quenched bcc phases have been defined.

* The extent of alternate metastable bcc phase nucleation and growth in the various alloys is strongly correlated to the calculated minimum amount of liquid undercooling required for bcc formation. With additions of bcc stabilizing elements to $NbCr_2$ (i.e., Nb, cr, and Ti), the metastable yield increases.

* The metastbale solidification pathwaysof the splat quenched alloys have been defined and correlated with the XRD results and microstructural analyses.

References

[56Elu]. V. P. Eluytin and V. F. Funke, Izv. Akad. Nauk. SSSR, Otd. Tekh. Nauk, 3 (1956) 68; Brutcher Trans. No. 4304, ASM, Cleveland, OH.

[58Ere]. V. N. Eremenko, G. V. Zudilova, and L. A. Gaevskaya, Metalloved. Term. Orab. Met. 1 (1958) 11; Brutcher Trans. No. 4108, ASM, Cleveland, OH.

[59Mis]. J. A. Misencik, Master's Thesis, MIT, (1959).

[61Gol]. H. J. Goldschmidt and J. A. Brand, J. Less-Common Met., vol. 3, p. 44, (1961).

[61Pan]. V. M. Pan, Dopov. Akad. Nauk Ukr. RSR, p. 332, (1961).

[65Ell]. R. P. Elliot, in "*Constitution of Binary Alloys, First supplement*", McGraw-Hill, New York, NY, p. 251, (1965).

[69Rud]. E. Rudy, Technical Report AFML-TR-65-2 Part V, p. 127, (1969).

[86Ven]. M. Venkatraman and J. P. Neuman, Bull. Alloy Phase Diag., vol. 7(5), p. 462, (1986).

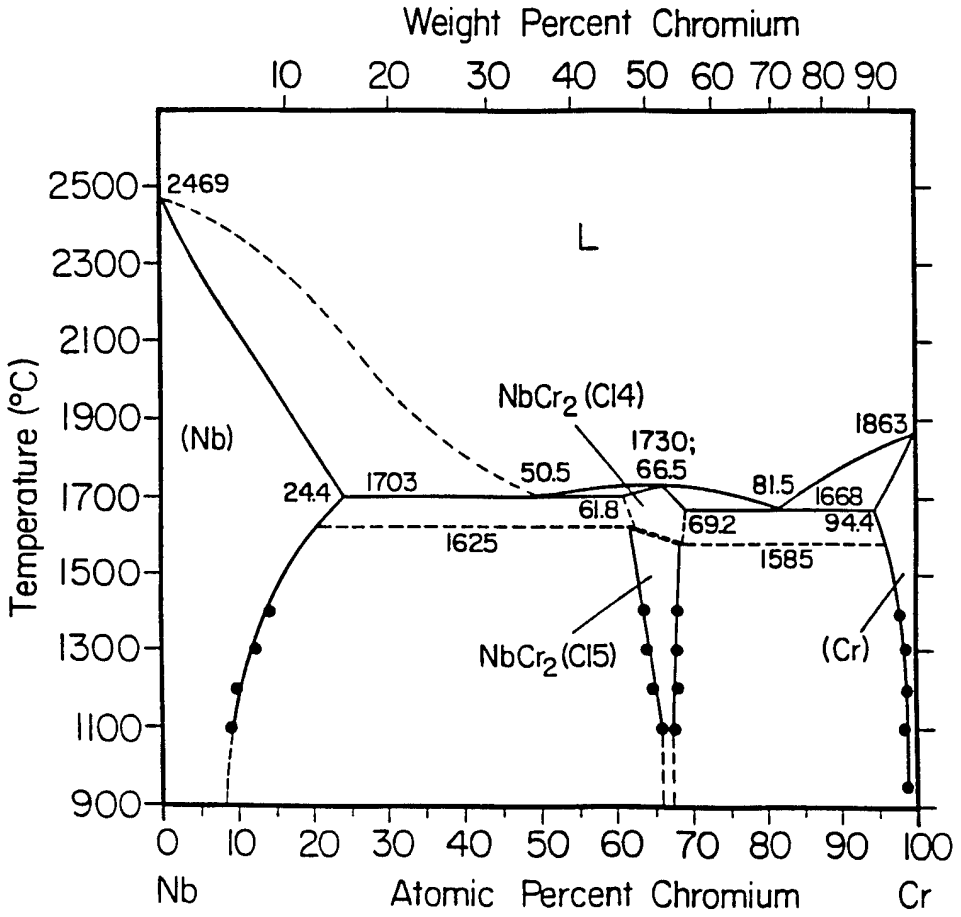

Figure 1. The Nb-Cr phase diagram constructed from the compositional data of the present study and the temperature values of references [61Pan,69Rud]. The solvus data points are from the quenching studies.

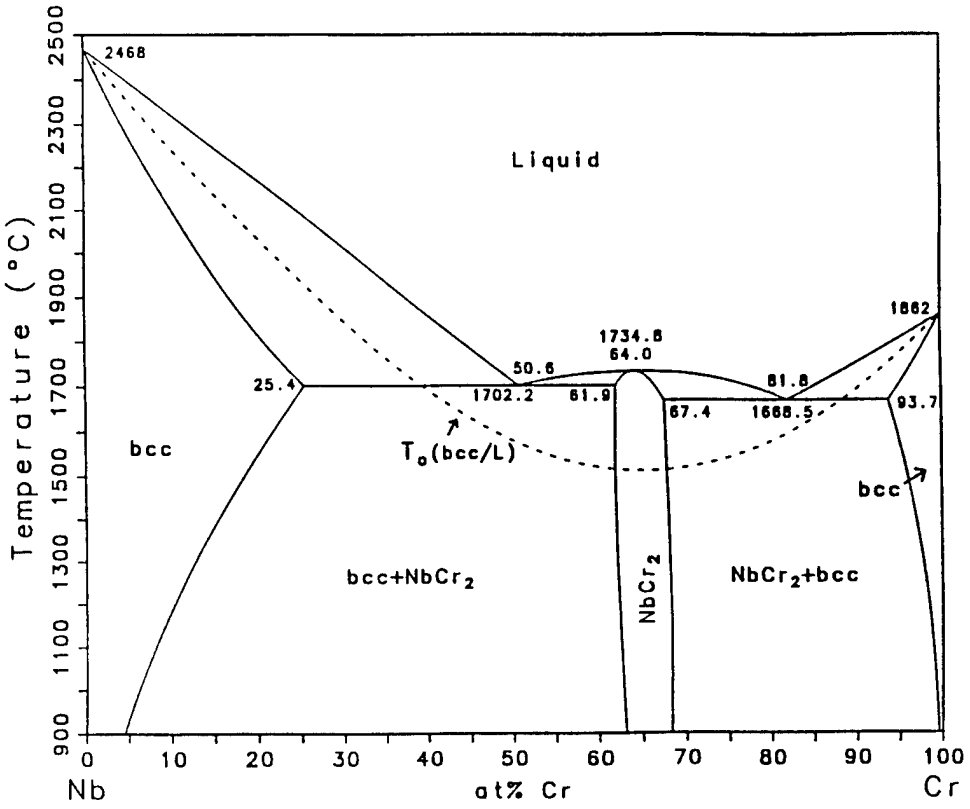

Figure 2. The calculated Nb-Cr phase diagram with T_O (bcc/L) curve.

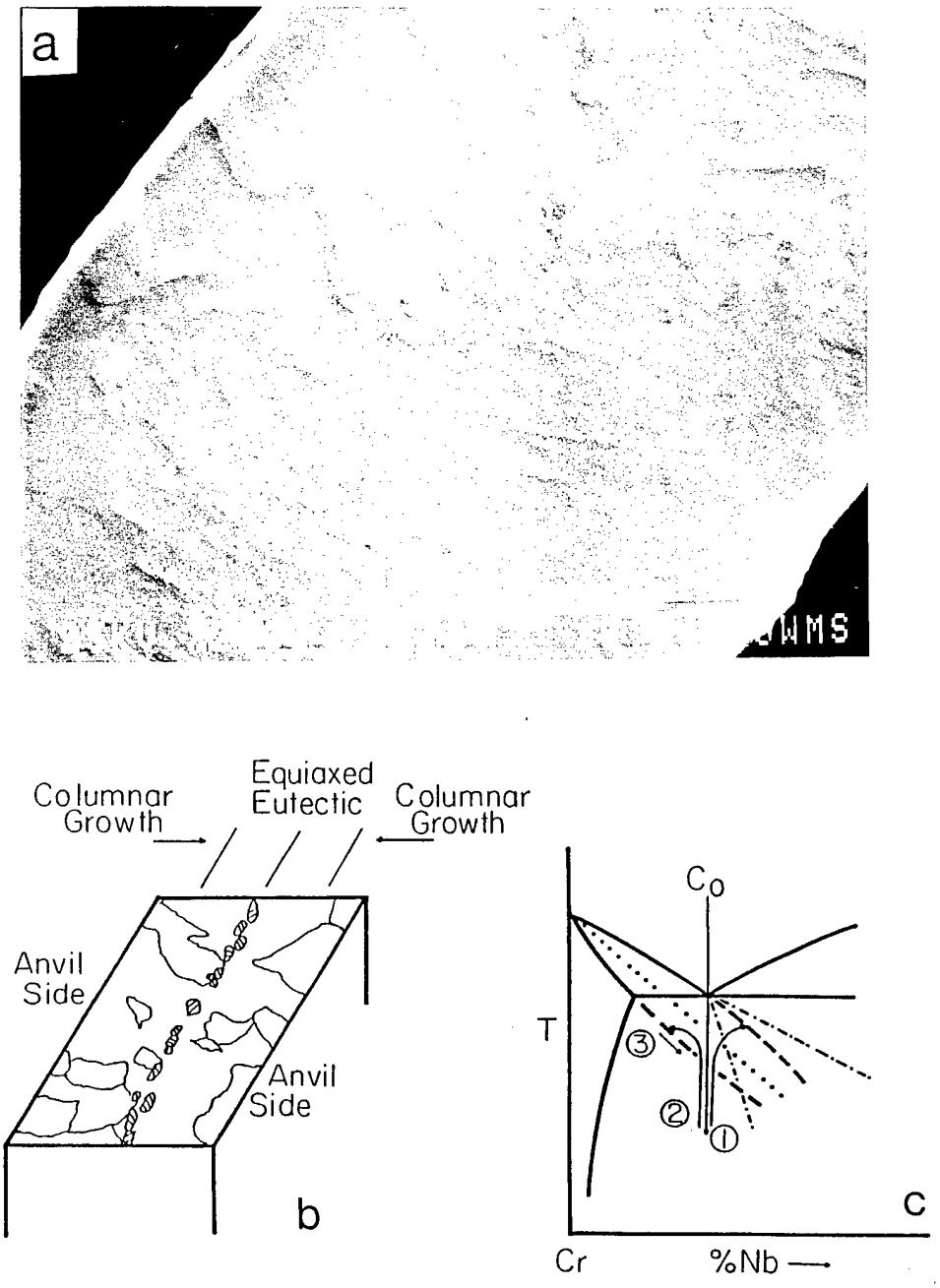

Figure 3. Microstructural development in a splat quenched Nb-82 at.% Cr sample where (a) SEM etched micrograph (b) schematic of microstructure and (c) solidification pathway.

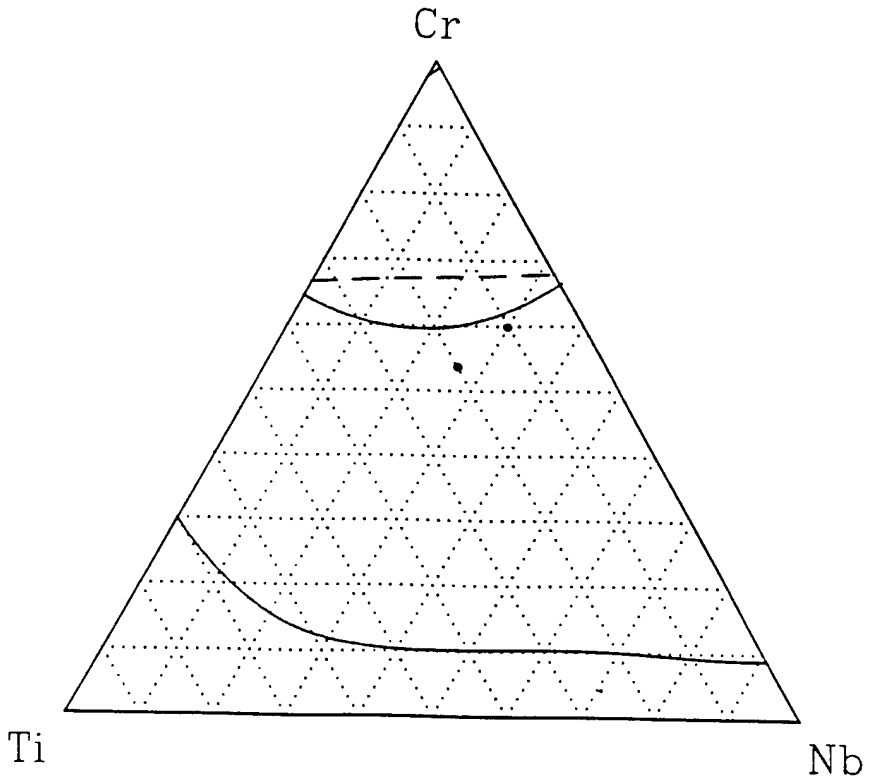

Figure 4. Nb-Cr-Ti ternary isotherm (950°C) illustrating the location of the $NbCr_2$-Ti plethal section alloys.

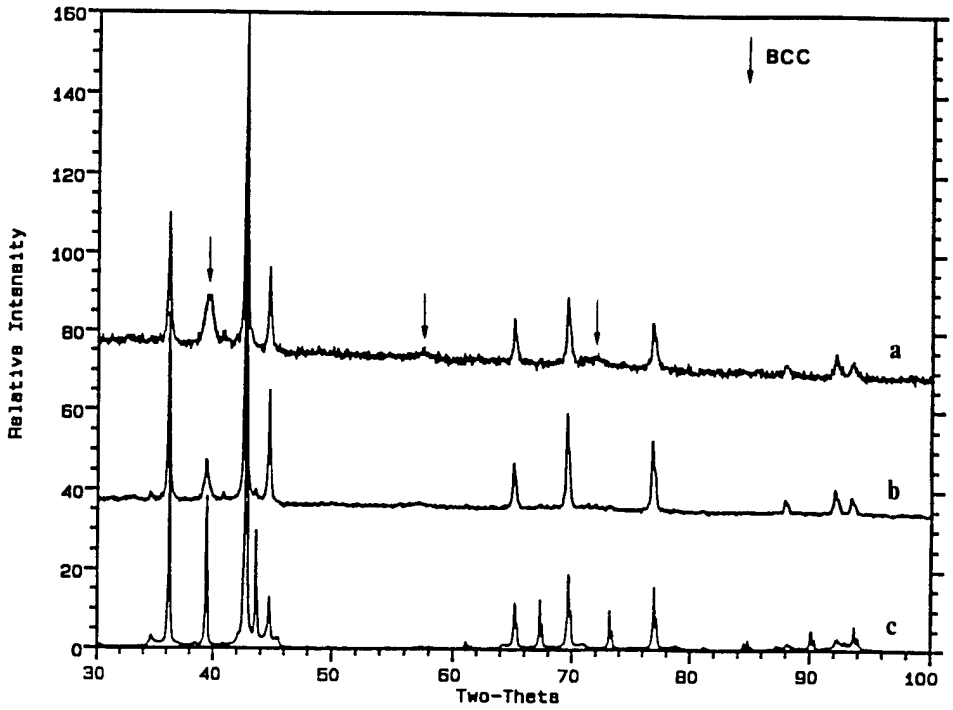

Figure 5. XRD traces of the arc-cast alloys along the $NbCr_2$-Ti plethal section where (a) 20 at.% Ti, (b) 10 at.% Ti, and (c) $NbCr_2$.

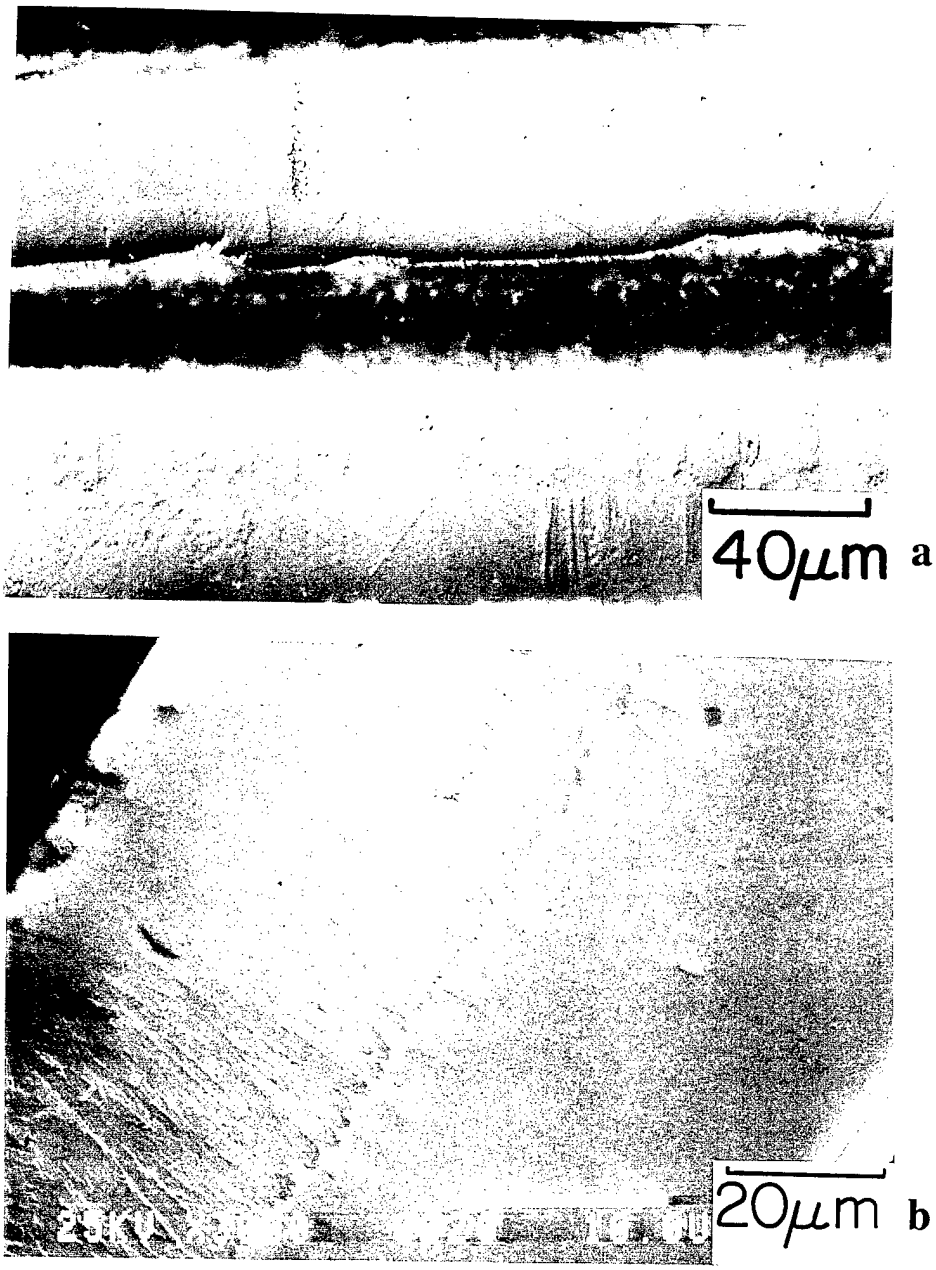

Figure 6. Micrographs of splat-quenched $NbCr_2$+10 at.% Ti samples where (a) optical etched and (b) SEM etched.

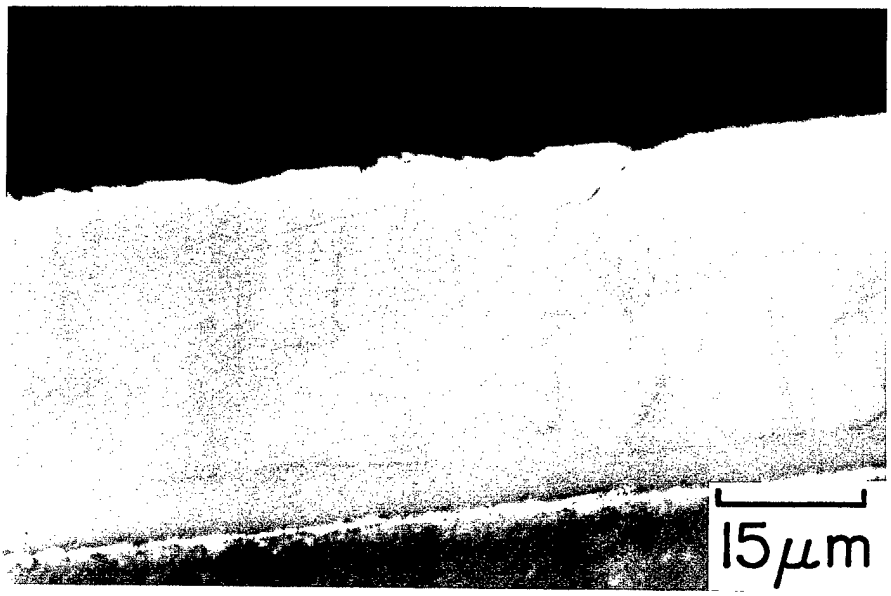

Figure 7. Optical micrograph (unetched) of a $NbCr_2$+20 at.% Ti sample.

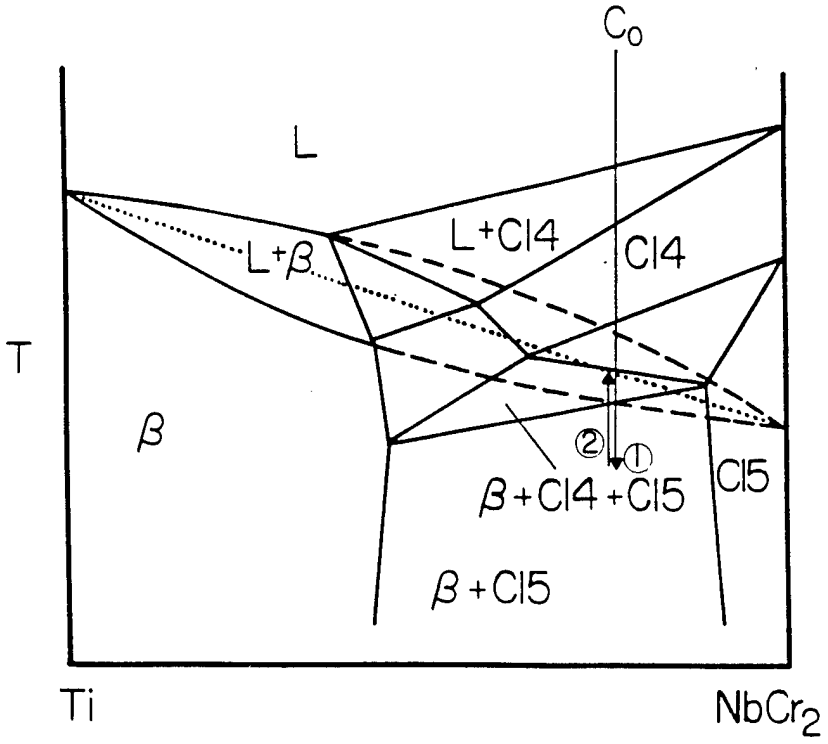

Figure 8. Schematic of solidification pathway in the $NbCr_2$+Ti splat-quenched samples.

V. Research Accomplishments in the Titanium Alloy/Al_2O_3 System

Metal matrix composites have become an important class of materials due to the need for low density materials with high strength and stiffness at elevated temperatures in advanced aerospace systems. The reinforcement of metals with ceramics causes an increase in strength, stiffness, wear resistance, high temperature strength, and a decrease in weight. At the same time, the chemical compatibility of matrix material with the reinforcing materials at high temperature is of major concern. The objective of this paper is to study the chemical compatibility of a metastable beta titanium alloy [TIMETAL 21S, Ti-15Mo-2.7Nb-3Al-0.2Si (wt.%)] with Al_2O_3. Alloy 21S has been chosen as a matrix material in the present study since its unique combination of properties makes it a viable candidate for high temperature metal matrix composite systems [90Ban,90Gra]. Alumina has been chosen as a reinforcing material in the present study although most of the works on titanium based composites have involved SiC fibers. The SiC fibers are known to react with the titanium alloys [85Rho] and so does the Al_2O_3 [473tre,91Mis]. But the coefficient of thermal expansion (CTE) mismatch between Al_2O_3 and titanium alloys are less compared to that between SiC and titanium alloys [90Kri]. Therefore, the thermal stress at the interface during cooling of a titanium alloy/Al_2O_3 composites will be considerably less than that developed in a titanium alloy/SiC composites. The possibility of using Nb as a diffusion barrier in the 21S/Al_2O_3 composite has also been investigated in this study.

In order to study the chemical compatibility between Al_2O_3 and 21S, a diffusion couple was prepared by hot pressing at 900^{o}C for 1 hour followed by slow cooling. Hot pressing was done just to develop a good bonding between the members of the diffusion couple. The diffusion couple was then clamped in an invar holder coated with Y_2O_3. The whole assembly was encapsulated in a quartz tube under vacuum and then annealed for long time (10 days at 900^{o}C) to establish the phase sequence at the interface. A back scattered SEM image of the interface of the diffusion couple and the corresponding concentration profiles (Ti, Al, Mo, Nb, and O) across the interface, as obtained from an electron microprobe are shown in figure 1. The

phases which are present in the reaction layer can be identified as γ-TiAl, α_2-Ti_3Al, and α-Ti(Al,O). The oxygen concentration, as determined by EPMA, should be used with caution due to the large errors generally associated with the quantitative analysis of light elements.

The reaction kinetics at 900°C has been studied. The kinetics of 21S/Al_2O_3 composite (AL_2O_3 fiber was HIP'd in 21S powder for 1 hour at 900°C under 15 ksi) has been compared with pure Ti, Ti-8Al-1Mo-1V, or Ti-6Al-2Sn-4Zr-2Mo/Al_2O_3 composites (figure 2). The reaction rate in 21S/Al_2O_3 system is much slower compared to the other systems, and this is probably due to the presence of heavy amount of alloying elements in 21S as suggested by Smith and Froes [84Smi]. The alloying of Ti with elements such as Mo reduces the activity of Ti, which in turn reduces the reaction rate significantly [84Smi]. One can calculate the activity of Ti in binary alloys from thermodynamic equations [80Bre,81Gas]. The activities of Ti in Ti-1.5 at.% Mo and Ti-9.5 at.% Mo alloys are 0.985 and 0.917, respectively. The activities at these two compositions have been calculated, since the amount of β stabilizing elements in Ti-8Al-1Mo-1V(wt.%) is 1.4 at.% (assuming V is equivalent to Mo) and in Ti-15Mo-2.7Nb-3Al-0.2Si (wt.%) is 9.5 at.% (assuming Nb is equivalent to Mo). Therefore, it appears that the reduction of activity of Ti (even by small amount) by alloying with elements such as Mo, V, etc., has significant effect in reducing the reaction rate.

Although the reaction rate is much slower in 21S/Al_2O_3 system, it is still severe enough to affect the mechanical properties of the composite material. In order to develop a strategy for a robust composite design, it is essential to prevent or at least decelerate the reaction kinetics at the interface. Suitable diffusion barrier can prevent reaction at the interface. The possibility of using Nb as diffusion barrier in 21S/Al_2O_3 composite has been investigated in this study. Niobium does not react with Al_2O_3 to form any reaction layer at the interface, although a small amount of Al from Al_2O_3 dissolves in Nb at a very high temperature [89Bur,89Mad]. The thermal expansion coefficients of Nb and Al_2O_3 are approximately same [89Bur,89Mad], and therefore, the thermal stress developed at Nb/Al_2O_3 interface during cooling from the bonding temperature would be very small, which in turn may increase the resistance to spalling and

cracking. Niobium is also the lightest of all the refractory metals. In order to evaluate the stability of Nb with 21S, a diffusion couple between Nb/21S was annealed at 1100°C for 100 hours. The composition profiles across the interface indicate that Nb diffuses into 21S (figure 3). Therefore, Nb will be depleted at long time if it is used as a diffusion barrier in the 21S/Al_2O_3 composite.

The optimum thickness of the Nb coating required to prevent the chemical reaction during the service lifetime of the composite can be determined from a diffusion analysis. Determination of the diffusivity of Nb in the multicomponent alloy 21S is a complicated task, but a first order calculation of the diffusivity of Nb in 21S has been done by Matano analysis [83She]. In determining the diffusivity of Nb, it has been assumed that the diffusivity of Nb is not influenced by other alloying elements (e.g., Mo and Al). This assumption is quite reasonable since the concentration profiles of Mo and Al remain basically unchanged by the diffusion of Nb (figure 3). The diffusivity of Nb at 1100°C and 1200°C are close to 2.0×10^{-10} cm^2/sec and 7.4×10^{-10} cm^2/sec, respectively. The activation energy as determined from the Arrhenius relationship, $D=D_0 \exp(-Q/RT)$ (where, D=diffusivity at temperature T, D_0=pre-exponential factor, Q=activation energy, R=gas constant), is 219 KJ/mol and the pre-exponential factor is 4.8×10^{-2} cm^2/sec. The calculated diffusivity at 900°C is close to 8.3×10^{-12} cm^2/sec. Using the calculated diffusivity at 900°C, the flux of Nb after 1 hour has been calculated and then the flux has been converted to equivalent thickness. This calculation suggests that a few micron thick (~2 μm) Nb can prevent the reaction at the interface during processing.

A piece of Al_2O_3 was coated with 2 μm Nb by the magnetron sputtering technique. Deposition was done at two pressure levels with periodic alterations between the high (7.0 to 7.4 mtorr) and low (2.8 to 2.9 mtorr) levels. This reduces the stress in the coating and ultimately prevents delamination of the coating from the Al_2O_3 substrate. A back scattered SEM image from the interface of a diffusion couple between Al_2O_3 (coated with 2 μm Nb) and alloy 21S (hot pressed at 900°C for 1 hour followed by annealing at 750°C for 110 hours) shows that Nb is able to prevent reaction at the interface (figure 4). Although coatings are able

to prevent reaction at the interface, one point of caution is that they are not always perfect. In that case, reaction may occur at that imperfection. An example is shown in figure 4 where discontinuous reaction layer (α_2) forms at the interface due to a coating imperfection (α_2 is shown by an arrow in the figure).

The service temperature of a composite is much lower than that of the processing temperature. The diffusion of Nb at the service temperature will be very slow. Therefore, one needs to be concerned about the Nb thickness which will be needed to prevent the reaction during the processing. If the processing condition varies between 850^{o}C to 900^{o}C for 2 hours, a few micron (2 μm) thick Nb coating will be able to prevent a reaction at the interface.

References

[90BAn]. P. J. Bania and W. M. Parris, in the proceedings of the 1990 TDA International Conference, Titanium Development Association, Dayton, OH, vol. 2, p. 784, (1990).

[90Gra]. J.S. Grauman, in the proceedings of the 1990 TDA International Conference, Titanium Development Association, Dayton, OH, vol. 1, p. 290, (1990).

[85Rho]. C. G. Rhodes and R. A. Spurling, in *Recent Advances in Composites in the United States and Japan*, eds., J. R. Vinson and M. Taya, ASTM, Philadelphia, PA, p. 585, (1985).

[73Tre]. R. E. Tressler and T. L. Moore, and R. L. Crane, J. of Mat. Sci., vol. 8, p. 151, (1973).

[91Mis]. A. K. Misra, Metall. Trans. A, vol. 22A, p. 715, (1991).

[90Kri]. S. Krishnamurthy, in *Interfaces in Metal-Ceramics Composites*, eds. R. Y. Lin, R. J. Arsenault, G. P. Martins, and S. G. Fishman, TMS, Warrendale, Pensylvania, p. 75, (1990).

[84Smi]. P. R. Smith and F. H. Froes, J. of Metals, March, p. 19, (1984).

[80Bre]. L. Brewer, R. H. Lamoreaux, R. Ferro, R. Marazza, K. Girgis, in *Atomic Energy Review*, Special Issue No. 7, ed. L. Brewer, IAEA, Vienna, Austria, (1980).

[81Gas]. D. R. Gaskel, in *Introduction to Metallurgical Thermodynamics*, second edition, McGraw-Hill, New York, NY, p. 362, (1981).

[89Bur]. K. Burger and M. Ruhle, Ultramicroscopy, vol. 29, p. 88, (1989).

[89Mad]. W. Mader and M. Ruhle, Acta. Metall., vol. 37, No. 3, p. 853, (1989).

[83She]. P. G. Shewmon, in *Diffusion in Solids*, J. Williams Book Company, Jenks, OK 74037, p. 29, (1983).

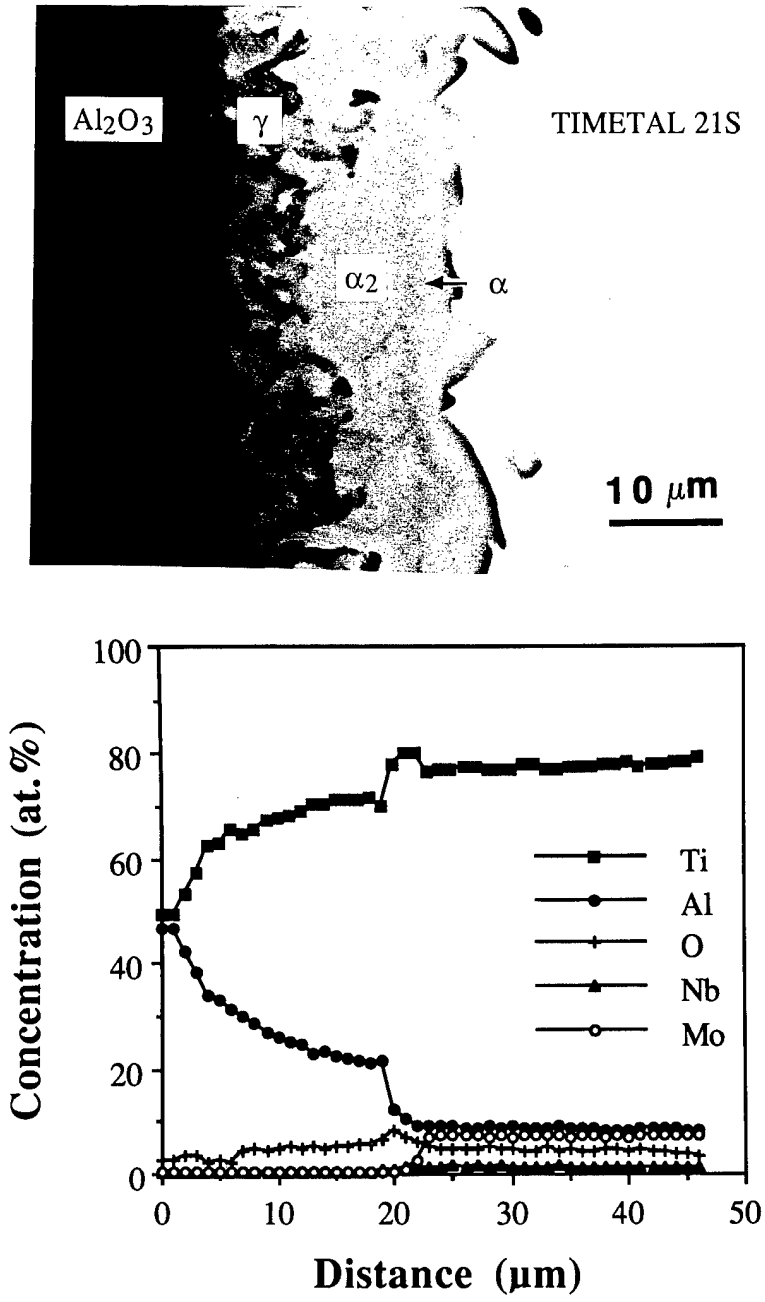

Figure 1. (a) Back scattered SEM image obtained from the interface of Al_2O_3/21S diffusion couple (hot pressed at 900°C for 1 hour and then annealed at 900°C for 242 hours) along with (b) composition profiles across the interface.

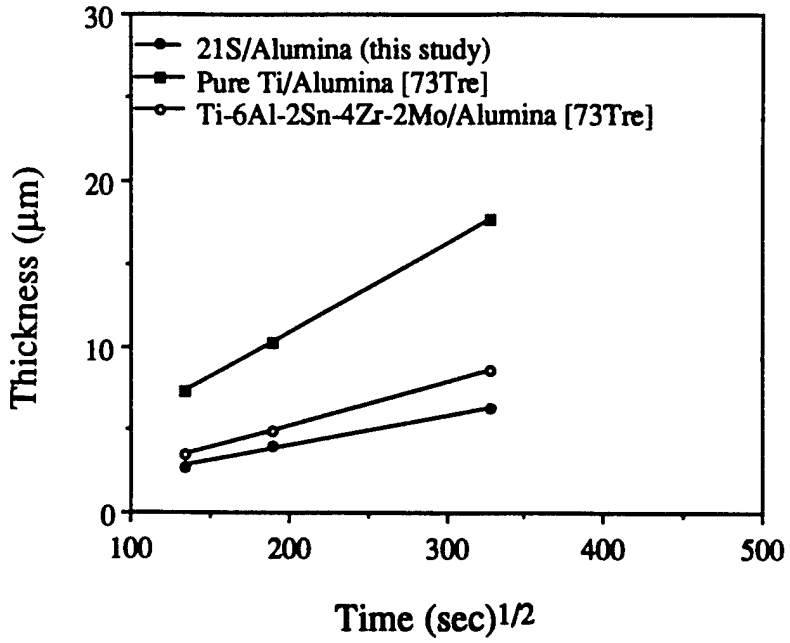

Figure 2. Reaction layer thicknes vs. $(time)^{1/2}$ plot for Pure Ti, Ti-6Al-2Sn-4zr-2Mo, or Ti-15Mo-2.7Nb-3Al-0.2Si/Al_2O_3 systems at 900°C.

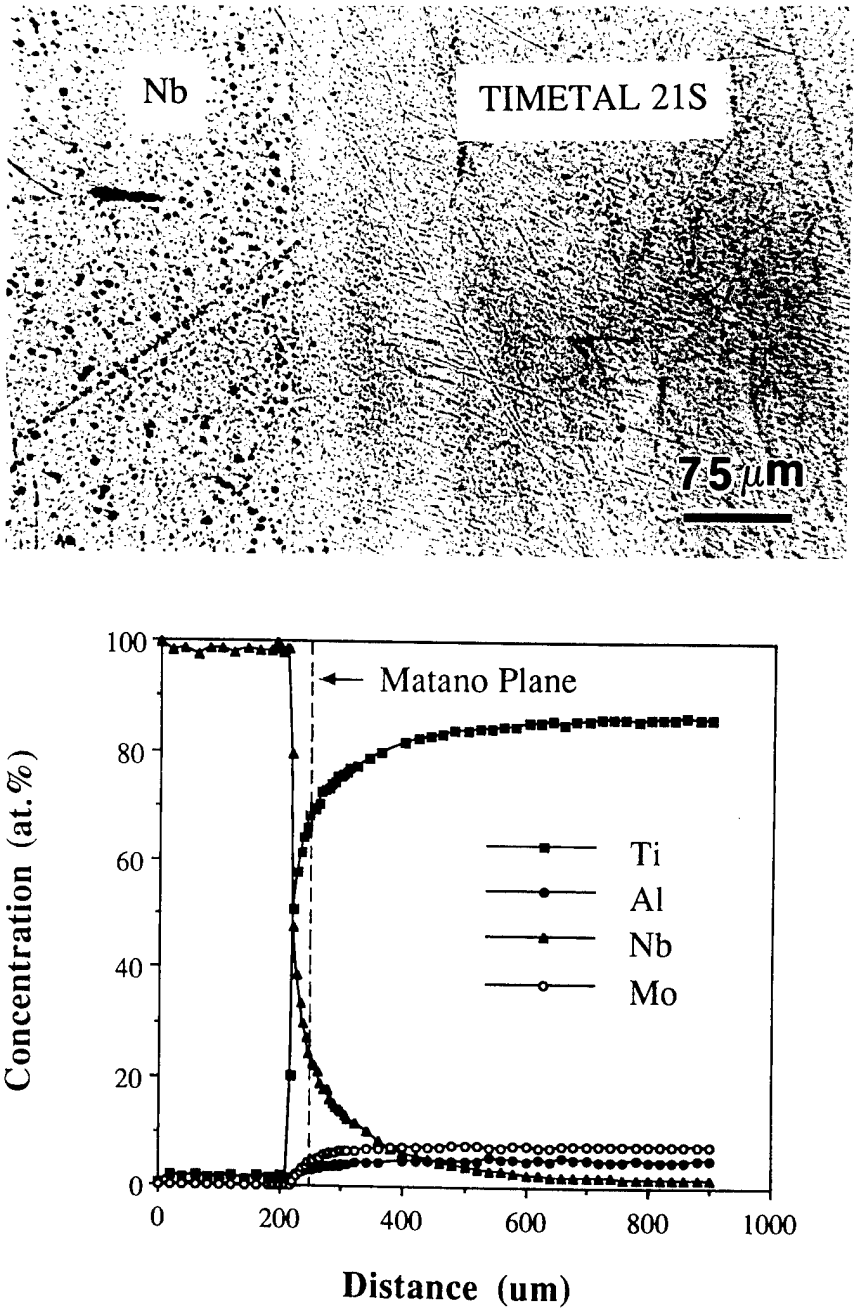

Figure 3. (a) An optical micrograph obtained from the interface of Nb/21S diffusion couple (annealed at 1100^{o}C for 100 hours) along with (b) composition profiles across the interface.

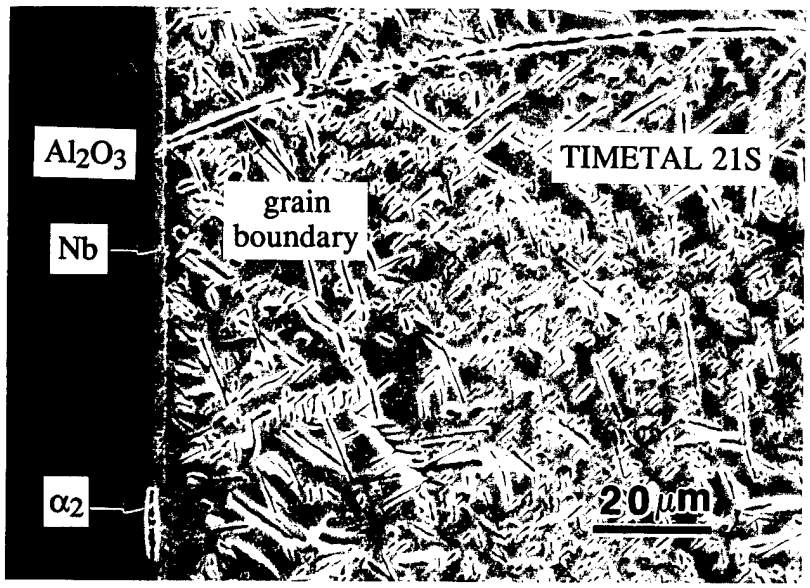

Figure 4. A secondary electron image obtained from the interface of Al_2O_3 coated with 2 μm Nb/21S diffusion couple (hot pressed at 900°C for 1 hour followed by annealing at 750°C for 111 hours) showing the formation of α_2-Ti_3Al at the interface.

VI. Research Accomplishments in the Titanium Alloy TIMWTAL 21S

A relatively new titanium alloy TIMETAL 21S (Ti-15Mo-2.7Nb-3Al-0.2Si-0.15O (in wt.%)) is a potential matrix material for advanced titanium matrix composites for elevated temperature use. In order to develop a perspective on the microstructural stability of this alloy, the influence of several commonly used heat treatments on the microstructure of TIMETAL 21S was studied using optical and transmission electron microscopy. Depending on the specific thermal treatment, a number of phases including α, ω-type, and silicide can form in this alloy. It was found that both recrystallized and non-recrystallized areas could be present in the microstructure of an annealed bulk alloy, but the microstructure of annealed sheet alloy was fully recrystallized. The mixed structure of the bulk alloy, developed due to inhomogeneous deformation, could not be removed by heat treatment alone at 900^{o}C. Athermal ω-type phase formed in this alloy upon quenching from the solution treatment temperature (900^{o}C). Silicide precipitates were also found in the quenched sample. Thermal analysis was used to determine the β transus and silicide solvus as close to 815^{o}C and 1025^{o}C, respectively. In solution treated and quenched samples, a high temperature aging at 600^{o}C resulted in the precipitation of α phase. The precipitation reaction was slower in the recrystallized regions compared to the non-recrystallized regions. During low temperature aging (350^{o}C) the ellipsoidal ω-type phase persisted in the recrystallized areas even after 100 hours, whereas a high density of α precipitates developed in the non-recrystallized area within only 3 hours. The observed behavior in precipitation may be related to the influence of substructure in the non-recrystallized areas providing for an enhanced kinetics during aging. The α precipitates (formed during continuous cooling from the solution treatment temperature, low temperature aging, and high temperature aging) always obeyed the Burgers orientation relationship. With respect to the microstructure, TIMETAL 21S is similar to other solute lean metastable beta titanium alloys.

VII. Publications of the Current Program

During a research program substantial time intervals often elapse between the completion of a research study, submission of a manuscript and the final appearance of a paper in print. As a result, the following list gives publications in preparation as well as those in print or press.

"Solidification Processing of $NbCr_2$ Alloys", D. J. Thoma and J. H. Perepezko, Mat. Res. Soc. Symp. Proc., vol. 194, p. 105, (1990).

"High Temperature Phase Stability in the Ti-Al-Nb System", J.H. Perepezko, Y.A. Chang, L.E. Seitzman, J.C. Lin, N.R. Bonda, T.J. Jewett and J.C. Mishurda in "High Temperature Aluminides and Intermetallics", Eds. S.H. Whang, C.T. Liu, D.P. Pope and J.O. Stiegler (TMS, Warrendale) p. 19, (1990)

" Decomposition Reactions and Toughening in NiAl-Cu Alloys", W.P. Allen, J.C. Foley, R.F. Cooper and J.H. Perepezko, Mat. Res. Soc. Symp. Proc. vol. 194, p. 405, (1990)

"High Temperature Phase Stability in the Ti-Al-Ta System", S. Das, T. J. Jewett, J. C. Lin, and J. H. Perepezko, in *Microstructure/Property Relationships in Titanium Aluminides and Alloys,* eds. Y-W. Kim and R. R. Boyer, TMS, Warrendale, PA, p. 31, (1991).

" Phase Stability and Processing of Titanium Aluminides", J.H. Perepezko, "Proceedings of Sixth International Symposium on Intermetallic Compounds", Ed. O. Izumi, The Japan Institute of Metals, p. 239, (1991)

"Phase Reactions and Processing in Ti-Al Based Intermetallics", J.H. Perepezko, ISIJ International vol. 31, p. 1080, (1991)

"Ternary Phase Development in the Ti-Al-Ta System," S. Das and J. H. Perepezko, Scripta Metallurgica et Materialia, vol. 25, p. 1193, (1991).

"Phase Stability and Solidification Pathways in $MoSi_2$ Based Alloys", P. S. Frankwicz and J. H. Perepezko, Mat. Res. Soc. Symp. Proc., vol. 213, p. 169, (1991).

"Phase Equilibria in Ti-Al Alloys", J. C. Mishurda and J. H. Perepezko, in *Microstructure/Property Relationships in Titanium Aluminides and Alloys,* eds. Y-W. Kim and R. R. Boyer, TMS, Warrendale, PA, p. 3, (1991).

"Alloy Phase Reactions near the Ti_2AlTa Composition," S. Das and J. H. Perepezko, in *Light Weight Alloys for Aerospace Applications II*, eds. E. W. Lee and N. J. Kim, TMS, Warrendale, PA, p. 453, (1991).

"High Temperature Phase Stability in Ternary Titanium Aluminides," J. H. Perepezko, T. J. Jewett, S. Das, and J. C. Mishurda, in the Proceedings of the 3rd. International SAMPE Metals and Metals Processing Conference, Toronto, Canada, SAMPE, Covina, CA, M357, (1992).

"Application of Ternary Phase Diagrams to the Development of $MoSi_2$-Based Materials," W. J. Boettinger, J. H. Perepezko, and P. S. Frankwicz, Mat. Sci. and Eng., vol. A155, p. 33, (1992).

"An Experimental Evaluation of the Phase Relationships and Solubilities in the Nb-Cr system," D. J. Thoma and J. H. Perepezko, Mat. Sci. and Eng., vol. A156, p. 97, (1992).

"Phase Stability of $MoSi_2$ with Cr Additions," P. S. Frankwicz and J. H. Perepezko, Mat. Res. Soc. Symp. Proc., vol. 288, p. 159, (1993).

" Phase Equilibria in the Titanium-Aluminum System", J.H. Perepezko and J.C. Mishurda, Titanium '92-Science and Technology, vol. 1, Eds. F.H. Fores and I. Kaplan, TMS, Warrendale, PA, p. 563, (1993)

"High Temperature Phase Equilibria of some Ternary Titanium Aluminides," S. Das, T. J. Jewett, and J. H. Perepezko, eds. R. Darolia, J. J. Lewandowski, C. T. Liu, P. L. Martin, D. B. Miracle, and M. V. Nathal, TMS, Warrendale, PA, p. 35, (1993).

"Phase Selection During Solidification Processing of Ti-40 at% Al Powder", E.M. Clevenger and J.H. Perepezko, Titanium '92-Science and Technology, vol. 1, Eds. F.H. Fores and I. Kaplan, TMS, Warrendale, PA, p. 571, (1993)

"Phase Stability and Alloy Design in High Temperature Intermetallics", J.H. Perepezko, "Critical Issues in High Temperature Structural Intermetallics", Eds. N.S. Stoloff, D.J. Duquette, A.F. Giamei, TMS, Warrendale, PA, p. 15, (1993)

"High Temperature Phase Equilibria in the Ti-Al-Ta Ternary system," T. J. Jewett, S. Das, and J. H. Perepezko, in *Titanium '92 Science and Technology*, eds. F. H. Froes and I. L. Caplan, TMS, Warrendale, Pa, vol. 1, p. 713, (1993).

"Development of a ($g+b_0$) Lamellar Microstructure in a $Ti_{45}Al_{50}Mo_5$ Alloy," S. Das, J. C. Mishurda, W. P. Allen, J. H. Perepezko, and L. S. Chumbley, Scripta Metallurgica et Materialia, vol. 28, p. 489, (1993).

"microstructural Study of the Titanium Alloy Ti-15Mo-2.7Nb-3Al-0.2Si (Timetal 21S)", K. Chaudhuri and J. H. Perepezko, Metall. and Materials Trans.A, vol. 25A, pp. 1109-18, (1994)

"Metastable BCC Phase Formation in the Nb-Cr System", D.J. Thoma, J.H. Perepezko, D.H. Plantz and R.B. Schwarz, Mat. Sci. and Engr. vol. A179/A180, p. 176, (1994)

"A Trijunction Diffusion Couple Analysis:", D.J. Thoma and J.H. Perepezko, "Experimental Methods of Phase Diagram Determination", Eds. J.E. Morral, R.S. Schiffmann and S.M. Merchant, TMS, Warrendale, PA, p. 45, (1994)

"Microstructural Stability", J.H. Perepezko, Intermetallic Compounds, vol. 1, Eds. J.H. Westbrook and R.L. Fleischer, J. Wiley, Sussex, UK, p. 849, (1994)

"Theoretical and Experimental Studies on the C15 Intermetallic Compound $NbCr_2$", F. Chu, D.J. Thoma, Y. He, T.E. Michtell, S.P. Chen and J.H. Perepezko, Mat. Res. Soc. Symp. Proc., vol. 364, p. 1089, (1995)

"A Geometric Solubility Analysis of Ranges in Laves Phases", D.J. Thomoa and J.H. Perepezko, Jnl Alloys and Compounds, vol. 224, p. 330, (1995)

"Metastable BCC Phase Formation in the Nb-Cr-Ti System", D.J. Thoma and J.H. Perepezko, Mats. Sci. Forum, vol. 179-181, p. 769, (1995)

"A High-Resolution Transmission Electron Microscopy Study of Interfaces Between the γ, B2 and α_2 phases in a Ti-Al-Mo Alloy, S. Das, J.M. Howe and J.H. Perepezko, Met. and Mat. Trans., vol. 27A, p. 1623, (1996)

VIII. Presentations

"Phase Equilibria in Ti-Al Alloys", TMS Fall Meeting, 1990

"High Temperature Intermetallic Alloys", ASM-Milwaukee Chapter, April 1991

"Update on Binary and Ternary Titanium Aluminide Phase Diagram", AeroMat 91, May 1991

"Phase Stability and Processing of Titanium Aluminides", Sixth International Symposium on Intermetallic Compounds, Sendai, Japan, June 1991

"Phase Relationships and Stabilities in the Nb-Cr and Nb-Cr-Ti Systems",TMS/ASM Fall Meeting in October 1991

"Application of Ternary Phase Diagrams to the Development of $MoSi_2$-Based Materials", First Int. Conf. On $MoSi_2$, November 1991

"Development of a (β_o+γ) Lamellar Microstructure in a $Ti_{45}Al_{50}Mo_5$ Alloy", TMS Annual Meeting, March 1992

"Phase Equilibria in the Ti-Al System", Seventh World Conf. On Ti, July 1992

"Phase Selection During Solidification Processing of Ti-40 at% Al Powder", Seventh World Conf. On Ti, July 1992

"High Temperature Phase Equilibria in the Ti-Al-Ta System", Seventh World Conf. On Ti, July 1992

"High Temperature Phase Stability in Ternary Titanium Aluminides", Third Int. SAMPE Metals Conf., October 1992

"High Temperature Phase Stability of $MoSi_2$", Fall TMS/ASM Meeting, November 1992

"Phase Stability and Alloy Design in High Temperature Intermetallics", Conference on Critical Issues in High Temperature Structural Intermetallics, Engineering Society/TMS Meeting, Kona Hawaii, March 1993

"Phase Stability of $MoSi_2$ with Cr Additions", Mat. Res. Soc. Symp., Boston, December 1993

"Metastable BCC Phase Formation in the Nb-Cr-Ti System", ISMANAM-94, Grenoble, France(1994)
"A Study of the B2/γ, B2/α_2, and α_2/γ Interfaces in the Ti-Al-Mo System", TMS 1994 Fall Meeting, Rosemont, Il

"The Stability of Al_2O_3 in Timet 21S", TMS 1994 Fall Meeting, Rosemont, Il

"Geometric Factors Affecting Solubility Ranges in Laves Phases", TMS 1995 Annual Meeting, Las Vegas

"In-Situ Composite Formation from Metastable Precursor Phases in the Nb-Cr-Ti System", TMS 1995 Annual Meeting, Las Vegas

IX. Participating Scientific Personnel

1) Professor J.H. Perepezko, Principal Investigator

2) Dr. S. Das, Postdoctoral Fellow

3) W.P. Allen, Ph.D (Completed 1990)

4) K. Chaudhuri, Ph.D (Completed 1994)

5) P.S. Frankwicz, Ph.D (Completed 1993)

6) T.J. Jewett, Ph.D (Completed 1993)

7) D.J. Thoma, Ph.D (Completed 1993)

8) E. Clevenger, M.S. (Completed 1991)

9) J.C. Mishurda, M.S. (Completed 1991)

10) C.B. Zimmermann M.S. (Completed 1994)